

Rotation Curves of High-Resolution LSB and SPARC Galaxies in Wave (Fuzzy) and Multistate (Ultra-light Boson) Scalar Field Dark Matter

T. Bernal,^{1*} L. M. Fernández-Hernández,^{1†} T. Matos^{2,3‡} and M. A. Rodríguez-Meza^{1,3§}

¹*Departamento de Física, Instituto Nacional de Investigaciones Nucleares, AP 18-1027, Ciudad de México 11801, México*

²*Departamento de Física, Centro de Investigación y de Estudios Avanzados del IPN, AP 14-740, Ciudad de México 07000, México*

³*Part of the Instituto Avanzado de Cosmología (IAC) Collaboration*

5th January 2017

ABSTRACT

Cold Dark Matter (CDM) has shown to be an excellent candidate for the dark matter of the universe at large scales, however it presents several difficulties with observations at the galactic level. On the other side, the Scalar Field Dark Matter (SFDM), also called Fuzzy, Wave, Bose-Einstein Condensate or Ultra-light Axion DM, is identical to CDM at cosmological scales but different at the galactic ones. Because of its quantum nature, the SFDM forms haloes with core density profiles; it has a natural cut-off in its matter power spectrum, thus it fits well the amount of satellite galaxies in the Milky Way neighbourhood, and predicts well-formed galaxies at high redshifts. In the recent years astronomers have measured the rotation curves and the amount of luminous matter and gas in galaxies with great accuracy. In this work we reproduce the rotation curves of high-resolution LSB and SPARC galaxies with two different SFDM profiles: (1) The soliton+NFW profile in the Wave DM (ψ DM) model, arising empirically from cosmological simulations of real, non-interacting SF at zero temperature, and (2) the multistate SFDM profile, an exact solution to the Einstein-Klein-Gordon evolution eqs. for a SF perturbation, taking into account the self-interaction and temperature of the real SF, introducing several quantum states as a realistic model for a SFDM halo. From the fits with the soliton+NFW profile, without assuming any cosmological restriction on the boson mass m_ψ , we obtained $0.264 < m_\psi/(10^{-23}\text{eV}/c^2) < 30.0$ and for the core radius $0.311 < r_c/\text{kpc} < 4.90$. Additionally we show the multistate SFDM model fits the observations better than the empirical soliton+NFW profile in a very simple way, even at the centres of the galaxies, and it reproduces naturally the wiggles present in some galaxies, being a theoretically motivated framework alternative to the ψ DM profile.

Key words: galaxies: haloes, galaxies: structure, (cosmology:) dark matter

1 INTRODUCTION

Dark matter (DM) was postulated first in order to explain the rotation curves of disk galaxies and the observed velocity dispersions in galaxy clusters, as well as the observational mass-to-light ratios in galaxies and clusters of galaxies (Zwicky 1933, 1937; Smith 1936; Rubin et al. 1980; Rubin 1983). Later, its necessity was evident to explain the gravitational lenses, the structure formation in the early universe, the acoustic baryonic oscillations, the power spectrum of galaxies, among other astrophysical and cosmological phenomena (see e.g. Bertone et al. 2005; Bennett et al. 2013). The space mission *Planck* has obtained the most precise map of the total matter-

energy content of the universe, setting the contribution of dark matter to $\sim 26\%$, meanwhile the baryonic matter is only $\sim 5\%$ and the cosmological constant Λ or dark energy is $\sim 69\%$ (Planck Collaboration et al. 2016).

The most accepted dark matter model is the Cold Dark Matter (CDM), which is very successful at reproducing the observations at cosmological scales; however, at the galactic level it faces some problems (see e.g. Weinberg et al. 2015). One of the difficulties is the so-called “cusp/core” problem, since from CDM N -body simulations the DM haloes are assembled with the “cuspy” Navarro-Frenk-White density profile (Navarro et al. 1997), which is proportional to $1/r$ at small radii and to $1/r^3$ at large distances, meanwhile many observations suggest a constant central density or “core” profile, e.g. in rotation curves of galaxies (Moore et al. 1999; de Blok et al. 2001a; McGaugh et al. 2007, 2016) and dwarf spheroidal (dSph) galaxies (Klypin et al. 1999; Kroupa et al. 2010;

* E-mail: tbernal@fis.cinvestav.mx

† E-mail: lfernandez@fis.cinvestav.mx

‡ E-mail: tmatos@fis.cinvestav.mx

§ Email: marioalberto.rodriguez@inin.gob.mx

Boylan-Kolchin et al. 2011; Walker 2013; Pawlowski et al. 2014). Another issue is the CDM prediction of too many satellite haloes around big galaxies like the Milky Way (Sawala et al. 2016) which have not been observed. Aside, it fails to reproduce the phase-space distribution of satellites around the Milky Way and Andromeda galaxies (Pawlowski et al. 2012; Ibata et al. 2013, 2014) and the internal dynamics in tidal dwarf galaxies (Gentile et al. 2007b; Kroupa 2012). Finally, another issue might lie in the early formation of big galaxies, since the CDM model predicts big galaxies were formed hierarchically from haloes less massive than $10^{12} M_{\odot}$, as is the typical case, but there are some recent observations of massive galaxies at very high redshifts ($5 \leq z < 6$) (Caputi et al. 2015).

Such problems at the galactic scales might be solved by introducing the baryonic physics to the simulations, which can be relevant at the centres of the galaxies and galaxy clusters through the inclusion, for example, of star formation, supernova explosions, stellar winds, active galactic nuclei, etc. (see e.g. Governato et al. 2010; Teyssier et al. 2013; Pontzen & Governato 2012; Madau et al. 2014; Di Cintio et al. 2014; Pontzen & Governato 2014). From a phenomenological point of view, empirical CDM density profiles have been proposed in order to explain the observations, e.g. the Burkert profile (Burkert 1996) and the generalised NFW profile (Zhao 1996). Aside, there are some alternatives to CDM seeking to solve the discrepancies at galactic scales without appealing to baryonic processes, for instance, Warm Dark Matter (Zavala et al. 2009; Navarro et al. 2010; Lovell et al. 2012), Self-Interacting Dark Matter (Spergel & Steinhardt 2000; Yoshida et al. 2000; Davé et al. 2001; Elbert et al. 2015) and Scalar Field Dark Matter (SFDM) (see Matos & Guzman 2000; Magaña et al. 2012; Suárez et al. 2014; Matos & Robles 2016; Marsh 2016; Hui et al. 2016, and references therein).

We are interested in the SFDM model, studied within some special cases and named differently depending on the authors. The motivation is the natural solution emerging from this model to the CDM problems mentioned before. The SFDM model assumes dark matter is a spin-0 scalar field (SF) ψ , with a typical ultra-light mass $m_{\psi} \sim 10^{-23} - 10^{-22} \text{ eV}/c^2$, which might include self-interactions. The first time when this idea was mentioned was in Baldeschi et al. (1983); since then the idea was rediscovered several times using different names (see e.g. Membrado et al. 1989; Press et al. 1990; Sin 1994; Ji & Sin 1994; Lee & Koh 1996; Matos & Guzman 2000; Sahni & Wang 2000; Peebles 2000; Goodman 2000; Matos & Ureña-López 2000, 2001; Hu et al. 2000; Wetterich 2001; Arbey et al. 2001; Boehmer & Harko 2007; Matos et al. 2009; Woo & Chiueh 2009; Bray 2010; Lundgren et al. 2010; Robles & Matos 2013b; Marsh et al. 2014; Schive et al. 014a) and more recently by Hui et al. (2016). However, the first systematic study of this idea started in 1998 by Guzman et al. (1999); Matos & Guzman (2000), showing that the observed rotation curves of disk galaxies can be reproduced by the SFDM model, and the cosmology was studied for the first time by Matos et al. (2000); Matos & Ureña-López (2000). Other systematic studies of the SFDM model were performed by Arbey et al. (2001); Arbey et al. (2002) and more recently by Marsh et al. (2014); Marsh (2016).

In the works by Matos et al. (2000); Matos & Ureña-López (2000), using the amount of satellite galaxies observed in the vicinity of the Milky Way, it was found that the mass of the scalar field should be $m_{\psi} \sim 10^{-22} \text{ eV}/c^2$. With this ultra-light mass, Alcubierre et al. (2002) found through numerical simulations that the gravitational collapse of a SF configuration forms stable objects with masses M of the order of a galaxy halo: $M \sim 10^{12} M_{\odot}$. Also,

with the characteristic ultra-light SF mass, the bosons condense very early in the universe at critical condensation temperatures of TeV (Matos & Ureña-López 2001), making up Bose-Einstein Condensates (BEC) interpreted as the dark matter haloes. One important property of the SFDM is that, at cosmological scales, it behaves as dust and reproduces the same observations as well as CDM: the cosmic microwave background and the mass power spectrum at large scales (Rodríguez-Montoya et al. 2010; Hlozek et al. 2015; Schive et al. 2016). Recently, Schive et al. (014a,b) have run high-resolution cosmological simulations of Scalar Field (Wave) DM and reproduced the same results.

In a series of papers (Matos & Ureña-López 2007; Bernal et al. 2008; Robles & Matos 2012) it was shown that the SFDM forms core haloes (see also Harko 2011). Further features of the SFDM were analysed, for example, the gravitational lensing was studied by Núñez et al. (2010); Robles & Matos (2013a); the ψ^4 -SF potential was studied by Matos & Suarez (2011); multistate solutions for the SF, i.e. bosons in excited states outside the ground energy level, have been considered (see e.g. Bernal et al. 2010; Robles & Matos 2013b; Martínez-Medina et al. 2015a; Bernal et al. 2016). Numerical simulations of galaxy formation were performed by Martínez-Medina & Matos (2014); Martínez-Medina et al. (2015b), where the characteristic spiral arms and bars of a disk galaxy were easily generated. It was also shown that satellite galaxies are stable around SFDM haloes (Robles et al. 2015). And a statistical study of high-resolution rotation curves of spiral galaxies in the BEC-DM model has been developed (Fernández-Hernández et al. 2016).

As mentioned before, the SFDM model has many variants, depending on the specific characteristic studied by different authors: the SF might be real or complex and possess a self-interaction, it might take into account also the temperature of the SF, by introducing a suitable SF potential. The model has been named as Fuzzy DM (FDM) (Hu et al. 2000), Wave DM (WDM or ψ DM) (Bray 2012; Schive et al. 014a) or Ultra-light Axion (ULA) DM (Hlozek et al. 2015); Bose-Einstein Condensate (BEC) DM (Boehmer & Harko 2007); Multistate SFDM (Robles & Matos 2013b), etc.

In the BEC-DM model (Boehmer & Harko 2007) it is assumed a dominant self-interaction between the particles (Thomas-Fermi limit); in this model all the bosons lie in the ground state at zero temperature; the mean boson mass from the analytic density profile is $m_{\psi} \sim 10^{-6} \text{ eV}/c^2$. This model has been widely studied, showing up sharp discrepancies in dwarf galaxies (Diez-Tejedor et al. 2014), disk galaxies (Boehmer & Harko 2007; Robles & Matos 2012; Fernández-Hernández et al. 2016) and galaxy clusters (Bernal et al. 2016), ruling out this approximation as a realistic SFDM model.

The first model studied in the present work is the Wave, Fuzzy or Ultra-light Axion DM, which share the same characteristics: a quadratic non-thermal, non-interacting potential with ultra-light masses $m_{\psi} \sim 10^{-23} - 10^{-21} \text{ eV}/c^2$. From the cosmological simulation by Schive et al. (014a,b), an empirical density profile was obtained for the Wave DM model, composed by a coupling of the asymptotic NFW decline with an inner soliton-like profile from the SFDM (“soliton+NFW” profile) (Schive et al. 014a; Marsh & Pop 2015).

Secondly, we investigate the multistate SFDM (Robles & Matos 2013b), which considers the SF is thermal at the very early universe, interacting with the radiation and the rest of matter. By introducing a self-interacting, temperature-corrected SF potential, the authors obtained an exact analytic solution for the SF density, including the ground and excited quantum states. This model has been proved successful in fitting the observations of dwarf spher-

oidal galaxies (Martínez-Medina et al. 2015a), the rotation curves of disk galaxies (Robles & Matos 2013b), the strong gravitational lensing (Robles & Matos 2013a) and the dynamical masses from X-ray observations of clusters of galaxies (Bernal et al. 2016).

In this work we reproduce the observed rotation curves of 18 high-resolution low surface brightness (LSB) galaxies, where only the DM is taken into account, 4 representative SPARC (Spitzer Photometry & Accurate Rotation Curves) galaxies and 2 other galaxies used in Robles & Matos (2013b) (the last 6 galaxies with high-resolution photometric information). For the galaxies with baryonic data, McGaugh et al. (2016); Lelli et al. (2016a) analysed 153 galaxies with the gas and stars information from the SPARC database (Lelli et al. 2016b), and found an empirical radial acceleration relation between the observed acceleration from the rotation curves of the galaxies and the acceleration from the baryonic component, showing a deviation at the value $g^\dagger = 1.2 \times 10^{-10} \text{ m/s}^2$. This result could suggest that baryons are the source of the gravitational potential, at least at small radii. As McGaugh et al. (2016) pointed out, such relation can be explained as the end product of galaxy formation processes (including the baryonic matter), new DM physics or the result of a modified gravity law. In the CDM paradigm, Ludlow et al. (2016) introduced different stellar and AGN feedback processes to explain the observed acceleration relation in well-resolved galaxies from the EAGLE simulation, showing that the empirical relation can be “accommodated” within the model. However, instead to look for complicated and diverse baryonic processes, in this work we test the two SFDM models with the observed rotation curves of some representative SPARC galaxies, showing that the model is consistent with the data.

The idea is to analyse statistically both approximations: the study can give us a clue for whether the scalar field is thermal or not, or if the self-interaction between SF particles can be important, assuming the scalar field is the dark matter of the galaxies. In order to do so, this work is organised as follows: In Section 2 we briefly explain the SFDM model and the two different approaches to be compared; in Section 3 we describe the galaxies’ samples used to fit the SFDM models; in Section 4 we present the results, and in Section 5 we discuss the results and present our conclusions.

2 SCALAR FIELD DARK MATTER

From particle physics motivation, spin-0 scalar fields are the simplest bosonic particles, described by the Klein-Gordon (KG) equation:

$$\square\psi - \frac{dV(\psi)}{d\psi} = 0, \quad (1)$$

for the real or complex scalar field ψ and the SF potential $V(\psi)$; from hereafter we use the notation $\hbar = 1 = c$, for c the speed of light and \hbar the reduced Planck’s constant. The scalar fields arise in cosmology to explain the inflationary epoch in the early universe and as alternatives to explain the accelerated expansion of the universe; they can describe also compact objects, as boson stars and supermassive black holes. As alternative to the CDM paradigm, it is proposed that DM haloes are constituted by ultra-light scalar fields, for which the complete Einstein-Klein-Gordon equations reduce to the Schrödinger-Poisson system in the Newtonian limit.

Until now, there is not an agreement on the correct form of the potential $V(\psi)$ for DM applications and some of them have been proposed in order to apply the SFDM theory to different astronomical and cosmological situations (see e.g. Suárez et al. 2014). A

general potential is given by

$$V(\psi) = \frac{1}{2}m_\psi^2\psi^2 + \frac{1}{4}\lambda\psi^4, \quad (2)$$

the so-called “double-well” potential, which includes the mass m_ψ of the SF and a self-interaction λ . For positive m_ψ^2 the potential has a single minimum at $\psi = 0$ and the potential is Z_2 invariant; for $-m_\psi^2$ the potential has two minima and the Z_2 symmetry appears spontaneously broken, being of great interest for physical situations (see Subsection 2.2). A recent study of large scale structure formation with the last potential has been developed by Suárez & Chavanis (2016). For this potential, in the hydrodynamic approach, it is possible to write an equation of state of the SF, resulting in a polytrope of index $n = 1$.

In the case $\lambda = 0$, the potential (2) reduces to

$$V(\psi) = \frac{1}{2}m_\psi^2\psi^2, \quad (3)$$

which has been widely used to model the SFDM in the universe, as discussed in the next Subsection.

2.1 Wave (Fuzzy) Dark Matter

The Fuzzy DM (FDM) (Hu et al. 2000), Wave DM (WDM) or ψ DM (Bray 2012; Schive et al. 014a) or Ultra-light Axion (ULA) DM (Hlozek et al. 2015) (here we name it as Schive et al. (014a), simply ψ DM), considers the SFDM is described by the potential (3), for ultra-light masses $m_\psi \sim 10^{-23} - 10^{-22} \text{ eV}$ and null self-interaction $\lambda = 0$. As showed by Matos & Ureña-López (2001); Schive et al. (014a); Ureña-López & González-Morales (2016), this approximation presents a cut-off in the power spectrum which suppresses the small scale structure formation below the de Broglie wavelength λ_{deB} (corresponding to halo masses $M < 10^8 M_\odot$ for $m_\psi \sim 10^{-22} \text{ eV}$), as a result of the quantum properties of the model (Heisenberg uncertainty principle), solving in this way the small scale structure overproduction in CDM. This approach assumes the SFDM is at zero temperature, implying all the bosons are in the ground state, i.e. the lowest energy level with no nodes. Also, Suarez & Matos (2011) showed that, within this approach, the evolution of perturbations of the SFDM model is identical to Λ CDM and Rodríguez-Montoya et al. (2010) showed the SFDM model is consistent with the acoustic peaks of the cosmic microwave background for a boson mass $m_\psi \sim 10^{-22} \text{ eV}$.

Nevertheless, Li et al. (2014) found that this model is not consistent with the Big Bang Nucleosynthesis (BBN) constraints for the boson mass m_ψ for any model with $\lambda = 0$, at 1σ -confidence level (CL), making necessary to introduce a self-interaction into the SF potential. Although their results allow to alleviate such restrictions at 2σ -CL, their work is a motivation to study a SF potential including a non-null self-interaction (see the next Subsection).

Schive et al. (014a,b) run a high-resolution cosmological simulation based on the dynamics of ψ DM in the Newtonian limit, governed by the Schrödinger-Poisson (SP) system. From the simulation, Schive et al. (014a) derived an empirical density profile for the DM haloes, consisting of a soliton-like core in every system, prominent before a transition radius, embedded in a NFW density halo, dominant at large radii. The motivation of this proposal is the expected loss of phase coherence of the ψ DM waves at large distances from the centre of distribution, expecting a transition from the soliton to the NFW profile (Marsh & Pop 2015). Such profile can be approximated by

$$\rho_{\psi\text{DM}}(r) = \Theta(r_\epsilon - r) \rho_{\text{sol}}(r) + \Theta(r - r_\epsilon) \rho_{\text{NFW}}(r), \quad (4)$$

where Θ is a step function, r_e is the transition radius where the density changes from the soliton profile (Schive et al. 014a):

$$\rho_{\text{sol}}(r) = \frac{\rho_c}{[1 + 0.091(r/r_c)^2]^8}, \quad (5)$$

to the NFW profile (Navarro et al. 1997):

$$\rho_{\text{NFW}}(r) = \frac{\rho_s}{(r/r_s)(1 + r/r_s)^2}. \quad (6)$$

In equation (5), $\rho_c := 1.9(m_\psi/10^{-23}\text{eV})^{-2}(r_c/\text{kpc})^{-4}M_\odot\text{pc}^{-3}$ is the central soliton density, m_ψ the boson mass and r_c the half-light radius of the soliton-like region. In equation (6), ρ_s is related to the density of the universe at the moment the halo collapsed and r_s is a scale radius. The total density profile (4) has 5 free parameters (m_ψ , r_c , r_e , ρ_s , r_s), which are reduced to 4 asking for continuity of the function at the transition radius r_e and up to 3 asking for differentiability at the same point (see Appendix A). Schive et al. (014a) found that the transition radius r_e is, in general, $r_e > 3r_c$.

There are several constraints on the boson mass m_ψ from different observations: From the study of the effect of tidal forces on the cold clumps in Ursa Minor, Lora et al. (2012) found $m_\psi \sim (0.3-1) \times 10^{-22}\text{eV}$, and in Sextants, Lora & Magaña (2014) found $m_\psi \sim (0.12-8) \times 10^{-22}\text{eV}$; from CMB and galaxy clustering data, Hlozek et al. (2015) constrained the mass $m_\psi > 10^{-24}\text{eV}$; from the high-redshift galaxy luminosity function, Schive et al. (2016) obtained $m_\psi > 1.2 \times 10^{-22}\text{eV}$; from Lyman- α observations, Sarkar et al. (2016) derived $m_\psi > 10^{-23}\text{eV}$. From ultra-faint dwarf spheroidal galaxies (dSphs) galaxies, Calabrese & Spergel (2016) derived $m_\psi \sim (3.7-5.6) \times 10^{-22}\text{eV}$.

For the classical dSph galaxies in the Milky Way, Marsh & Pop (2015) constrained m_ψ using the soliton+NFW density profile (4), through stellar populations' observations in Fornax and Sculptor and found $m_\psi < 1.1 \times 10^{-22}\text{eV}$. More recently, Chen et al. (2016) applied the Jeans analysis to the kinematic data of the eight dSphs to constrain m_ψ ; for all the dSphs, except for Fornax, as the transition radii are outer the half-light radii r_c , they took into account the soliton core profile (5) only, deriving a mass $m_\psi = 1.18 \times 10^{-22}\text{eV}$. For Fornax, they applied the complete density profile (4) and found a larger $m_\psi = 1.79 \times 10^{-22}\text{eV}$ and smaller r_c , with respect to the soliton-only model results. Most recently, González-Morales et al. (2016) constrained m_ψ with the complete soliton+NFW profile (4), using kinematic mock data of Fornax and Sculptor, which include the stellar components of the galaxies, finding core radii $r_c > 1.5\text{ kpc}$ and $r_c > 1.2\text{ kpc}$, respectively, and $m_\psi < 4 \times 10^{-23}\text{eV}$. Such results are in tension with the estimates from the cold clumps in Ursa Minor and Sextants (Lora et al. 2012; Lora & Magaña 2014), the high-redshift luminosity function (Schive et al. 2016) and the ultra-faint dSphs studies (Calabrese & Spergel 2016). González-Morales et al. (2016) suppose that such small boson mass might be the result of baryonic feedback processes present in the dSph galaxies.

For the LSB and SPARC galaxies analysed in the present work, we assume the soliton+NFW profile (4) for the ψ DM model and expect the transition radius r_e is well inside the radius of the last observed point (spanning a range $R_{\text{max}} \sim 1-30\text{ kpc}$, for the maximum radius of luminous matter), thus we apply the complete density profile. Additionally, we impose continuity and differentiability conditions to the total profile at the transition radius r_e , assuming a smooth transition between the soliton and the external NFW halo. With these two additional conditions, it is possible to write the NFW parameters r_s and ρ_s in function of the other three

free parameters, thus we fit only m_ψ , r_c and r_e . The complete expressions are written in Appendix A.

2.2 Multistate Scalar Field Dark Matter

As a step forward on the study of the SFDM model, Robles & Matos (2013b) considered the general double-well potential (2), with a no-null self-interaction term, plus one-loop finite-temperature T corrections (Kolb & Turner 1994):

$$V(\psi) = -\frac{1}{2}m_\psi^2\psi^2 + \frac{1}{4}\lambda\psi^4 + \frac{1}{8}\lambda\psi^2T^2 - \frac{\pi^2}{90}T^4, \quad (7)$$

in units $k_B = 1$ for the Boltzmann constant and where the Z_2 symmetry appears spontaneously broken (with the term $-m_\psi^2$). Such self-interacting, finite-temperature corrected potential is motivated by the theoretical expectation of modern particle physics that, at high temperatures, symmetries spontaneously broken today were restored. Symmetry breaking studies are of great interest for diverse physical situations, assuming the universe has underwent phase transitions during its evolution (see e.g. Kolb & Turner 1994, and references therein), as for example, the inflationary era. With this motivation in mind, Robles & Matos (2013b) consider that at the very early universe, the initial SF fluctuations from inflation interact with the rest of matter and radiation at very high temperatures $T \gg T_c$, for T_c the critical temperature where $\psi=0$ is a minimum of the potential and the symmetry is restored. In this case, the SF is embedded in a thermal bath at finite temperature T at very early times¹. As the universe expands, the temperature decreases and eventually the SF decouples from the rest of matter, evolving independently. As the potential (7) depends on the 4th-power with respect to T , as the temperature continues decreasing, the SF goes through a Z_2 spontaneous symmetry breaking (SSB), which turns a minimum of the potential to a maximum, which increases the amplitude of the initial SF perturbations forming the initial galaxy haloes (see also Matos & Rodríguez-Meza 2014, for the study of the SSB of a charged complex SF).

For cosmological applications, Robles & Matos (2013b) assumed the SSB at $T=T_c$ takes place in the radiation dominated era. They found that at that moment the SF fluctuations can start growing in the linear regime for $T < T_c$, until they reach a new stable minimum. Then obtained the perturbed Einstein-Klein-Gordon evolution equations for the SF perturbation, $\delta\psi$, in a Friedmann-Lemaître-Robertson-Walker background spacetime. Under these assumptions, the galactic haloes could have been formed almost at the same time of the SSB and with similar masses, $M \sim 10^{12}M_\odot$ (for $m_\psi \sim 10^{-22}\text{eV}$), which is the typical mass of a galaxy like ours. Later on, such haloes can enter in the non-linear regime, merging and constituting larger structures, hierarchically, just like in the CDM model.

Under the linear approximation to describe the evolution of a galaxy halo, in the Newtonian regime, the exact solution to the perturbation equations for the temperature-corrected potential (7) is found as (Robles & Matos 2013b)

$$\rho_{\text{SFDM}}^j(r) = \rho_0^j \left[\frac{\sin(k_j r)}{(k_j r)} \right]^2; \quad (8)$$

thus the finite-temperature corrected potential (7) implies the existence of different excitation states j as solution to the SF perturbation equation, i.e. the bosons are thermally distributed in the ground

¹ In equation (7), the term $\propto \psi^2 T^2$ appears due to the interaction of the SF with the thermal bath and the term $\propto T^4$ is due to the thermal bath only.

and excited states at higher energy levels, and the general solution allows a configuration out of the fully condensate system. In the last equation, $j = 1, 2, 3, \dots$ is the number of the excited state required to fit the mass distribution, $\rho_0^j = \rho_{\text{SFDM}}^j(0)$ is the central density and the radius R of the SF configuration is fixed through the condition $\rho_{\text{SFDM}}^j(R) = 0$, i.e. $k_j R = j\pi$. This solution is naturally core. The mass distribution is given by

$$M_{\text{SFDM}}^j(r) = \frac{4\pi G \rho_0}{k_j^2} \frac{r}{2} \left[1 - \frac{\sin(2k_j r)}{(2k_j r)} \right]. \quad (9)$$

Now, as the solution to the SF perturbation equation is linear, it is possible to have combinations of excited states; this means that the total density ρ_{SFDM} can be written as the sum of the densities in the different excited states (Robles & Matos 2013b):

$$\rho_{\text{SFDM}}(r) = \sum_j \rho_0^j \left[\frac{\sin(j\pi r/R)}{(j\pi r/R)} \right]^2. \quad (10)$$

It is worth noting that the radius R in the last equation is the same for all the excited states present in the configuration and it is defined as the radius of the SFDM halo. Such profile has at least two free parameters for one state and every additional excited state adds one parameter, ρ_0^j . The disadvantage of this profile is that the physical parameters of the SF, m_ψ and λ , are degenerated with other quantities, like the critical temperature T_c at the SSB, the temperature of the halo at the formation time, etc. However, this model has been proved successful in fitting the observations of dwarf spheroidal galaxies (Martinez-Medina et al. 2015a), the rotation curves of galaxies (Robles & Matos 2013b), the dynamical masses from X-ray observations of clusters of galaxies (Bernal et al. 2016), predicting the size of the Einstein radius of lensed galaxies by strong gravitational lensing (Robles & Matos 2013a) and the survivability of satellite SFDM haloes orbiting around a Milky Way-like galaxy (Robles et al. 2015).

3 GALAXIES' SAMPLES

3.1 High-Resolution LSB Galaxies

We are using two sets of galaxy rotation curves according to the availability of photometric data. For the low surface brightness (LSB) galaxies, in which the dark matter is the dominant component, we are using the observed rotation curves of 18 high-resolution LSB galaxies reported in de Blok et al. (2001a). In this work, the authors considered the visible data contribution, classifying the galaxies according with the availability of photometric data and using three models: the minimum disk model, where the dark matter is the principal component in the haloes, making zero all the visible components for the galaxies with photometry, a constant M/L_* and the maximum disk models where only the galaxies with photometry data are considered.

Given that we are interested in testing dark matter models the set without photometric data will be used. This set is in Table 1, where we describe some important characteristics of each galaxy.

3.2 NGC galaxies with photometric data

In this work we selected, as representative systems of the second set of galaxies with photometric data, the three sample galaxies in McGaugh et al. (2016) (NGC 7814, 6503, 3741) from the SPARC (Spitzer Photometry & Accurate Rotation Curves) database (Lelli et al. 2016b), and the sample galaxies used in Robles & Matos

(2013b) (NGC 1003, data from SPARC; NGC 1560, data from de Blok et al. (2001b); NGC 6946, data from McGaugh (2005)). In Table 2 we show the characteristics of these galaxies.

The SPARC database contains the near-infrared photometry (tracing the stellar mass distribution) and high-resolution HI/H α rotation curves (tracing the gravitational potential out to large radii) of 175 disk galaxies, deriving with high resolution the stellar and gas components of the galaxies (Lelli et al. 2016b). The sample represents a wide range in morphological types, stellar masses, surface brightnesses and gas fractions, and the mass models are reconstructed from the observed distributions of stars and gas for different characteristic radii and values of the stellar mass-to-light ratio. The database includes low surface brightness (LSB) galaxies, in major part gas-dominated dwarf galaxies; high surface brightness (HSB) galaxies, in major part bulge-dominated spiral galaxies; and intermediate surface brightness (ISB) galaxies, which are disk-dominated systems.

Usually, in LSB galaxies the dark matter component is dominant even at small radii, whilst in HSB galaxies the contribution of the stellar and gas components to the total mass is important at the central regions. However, McGaugh et al. (2016) found that, even when the dark matter is dominant at the inner regions for many galaxies, the observed acceleration in 153 galaxies of all types (LSB, ISB and HSB galaxies) from the SPARC database strongly correlates with the acceleration from the baryonic matter, showing a mass discrepancy at the value $g^\dagger = 1.2 \times 10^{-10} \text{ m/s}^2$. Therefore, in this work, we investigate the consistency of the two SFDM models with the observational rotation curves of four representative SPARC galaxies, including the baryonic information.

3.3 Statistical calibration method

The galaxy rotation curve is given by

$$V(r) = \sqrt{\frac{GM_T(r)}{r}}, \quad (11)$$

where $M_T = M_{\text{bulge}} + M_{\text{disk}} + M_{\text{gas}} + M_{\text{DM}}$, for M_{DM} the dark matter contribution depending on the density profile used (soliton+NFW or multistate SFDM). In the case of the LSB galaxies (Subsection 3.1), $M_T = M_{\text{DM}}$, and for the galaxies with photometric information (Subsection 3.2) we consider the different baryonic components (bulge, disk-stars and gas), if given.

In order to constrain the free parameters of every SFDM model, we used the Markov Chain Monte Carlo (MCMC) method (Gelmanman 1997), through a maximisation of the likelihood function $\mathcal{L}(\mathbf{p})$ given by

$$\mathcal{L}(\mathbf{p}) = \frac{1}{(2\pi)^{N/2} |\mathbf{C}|^{1/2}} \exp \left(-\frac{\Delta^T \mathbf{C}^{-1} \Delta}{2} \right), \quad (12)$$

where \mathbf{p} is the vector of parameters, N the number of observational points for each galaxy, $\Delta = V_{\text{obs}}(r_i) - V_{\text{model}}(r_i, \mathbf{p})$, for V_{obs} the observational circular velocity at the radius r_i and V_{model} the derived total velocity for a given SFDM model computed in the same position where V_{obs} was measured, and \mathbf{C} a diagonal matrix.

We sample the parameter space from uniform prior ranges with two Markov chains and tested the convergence of the fit with the Gelman-Rubin convergence criterion ($\mathcal{R} - 1 < 0.1$) (Gelman & Rubin 1992). The fitting parameters and 1σ and 2σ confidence ranges are computed from the Markov chains with 30% as burn-in.

Simultaneously, we used the data analysis software *ROOT* (Brun & Rademakers 1997). The method minimises the χ_{red}^2 er-

High-resolution LSB galaxies					
Galaxy Name (1)	Morphology (2)	M_{abs} (mag) (3)	R_{max} (kpc) (4)	V_{max} (km/s) (5)	D (Mpc) (6)
ESO-LV 014-0040	Spiral	-21.6	29.2	263	212
ESO-LV 084-0411	Edge-on	-18.1	8.9	61	80
ESO-LV 120-0211	Fuzzy Magellanic bar	-15.6	3.5	25	15
ESO-LV 187-0510	Irregular spiral, flocculent	-16.5	3.0	40	18
ESO-LV 206-0140	Spiral	-19.2	11.6	118	60
ESO-LV 302-0120	Spiral, hint of bar?	-19.1	11.0	86	69
ESO-LV 305-0090	Barred spiral	-17.3	4.8	54	11
ESO-LV 425-0180	Spiral	-20.5	14.4	145	86
ESO-LV 488-0490	Inclined Magellanic bar	-16.8	6.0	97	22
F730-V1	Spiral	...	11.9	145	144
UGC 4115	Im	-12.4	1.0	40	3.2
UGC 11454	Fuzzy spiral, small core	-18.6 ^a	11.9	152	91
UGC 11557	SBdms	-20.0	6.2	95	22
UGC 11583	dI	-14.0 ^a	1.5	36	5
UGC 11616	Sc	-20.3 ^a	9.6	143	73
UGC 11648	I	-21.0 ^a	12.7	145	48
UGC 11748	Sbc	-22.9 ^a	21.0	242	73
UGC 11819	dG	-20.3 ^a	11.7	153	60

Table 1. In this Table we show the characteristics of the 18 high-resolution LSB galaxies (de Blok et al. 2001a) used in the present work. The columns read: (1) The name of the galaxy, (2) Morphology, (3) Absolute magnitude (^a is Zwicky magnitude 17), (4) Maximum observational radius, (5) Maximum velocity of the rotation curve and (6) Distance to the galaxy.

Galaxies with photometric data					
Galaxy Name (1)	Morphology (2)	M_{abs} (mag) (3)	R_{max} (kpc) (4)	V_{max} (km/s) (5)	D (Mpc) (6)
NGC 7814 ^a	Sabl	-20.15 ^d	5.03	218.9	14.40
NGC 6503 ^a	Scd	-17.7 ^e	3.04	116.3	6.26
NGC 3741 ^a	Im	-13.13 ^f	5.14	50.1	3.21
NGC 1003 ^a	SA(s)cd	-19.2	31.3	115	11.8
NGC 1560 ^b	Sd	-15.9	8.3	78	3.0
NGC 6946 ^c	SABcd	—	—	224.3	10.1

Table 2. The same as Table 1 for the galaxies with photometric data.

^aData from the SPARC database (Lelli et al. 2016b).

^bData from de Blok et al. (2001b).

^cData from McGaugh (2005).

^dMonachesi et al. (2016).

^eKoda et al. (2015).

^fGentile et al. (2007a); Dutta et al. (2009).

rors to obtain the best fit from the observations:

$$\chi_{\text{red}}^2 = \sum_{i=1}^N \left(\frac{V_{\text{obs}}(r_i) - V_{\text{model}}(r_i, \mathbf{p})}{\sigma_i} \right)^2, \quad (13)$$

where σ_i is the error in the measurement of $V_{\text{obs}}(r_i)$.

4 RESULTS

In this Section we show the results of the fits with the two SFDM models. In Subsection 4.1 we present the results for the ψ DM model with the soliton+NFW density profile (4), separately for the high-resolution LSB galaxies (Subsection 4.1.1) and for the galaxies with photometric information (Subsection 4.1.2). In Subsection 4.2 we show the results for the multistate SFDM model

with the density profile (10), also separating the fits with the high-resolution LSB galaxies (Subsection 4.2.1) and the galaxies with photometric data (Subsection 4.2.2).

4.1 Soliton+NFW fits

4.1.1 High-resolution LSB galaxies

Table 3 shows the results for the 18 high-resolution LSB galaxies reported in de Blok et al. (2001a), for the ψ DM model with the soliton+NFW density profile (4). As explained in Appendix A, we restricted the density profile asking for continuity and differentiability of the function (4) at the transition radius r_ϵ , as a smooth transition between the soliton and NFW regions. With these restrictions we have three free parameters: the central density ρ_c , the soliton-like core radius r_c , and the transition radius r_ϵ . We report the 1σ errors from the MCMC method used, also the reduced χ_{red}^2 errors for each galaxy. From ρ_c and r_c we obtained the boson mass m_ψ , and with r_ϵ we computed the NFW parameters, r_s and ρ_s (see Appendix A), and additionally, derive the virial radius r_{200} and concentration parameter $c := r_{200}/r_s$,² shown in the same Table.

Figure 1 shows the resulting plots for the density profile (4) for the fitting parameters shown in Table 3; the transition radius r_ϵ is the vertical line shown for all the galaxies. The observational error bars are big for some galaxies in the sample and, in general, the fits are good, except at the outer region of UGC11748. Figure 2 shows the 1σ and 2σ contours for the parameters m_ψ and r_c from the MCMC analysis, and the transition radius r_ϵ is the scatter coloured plot.

From Table 3 it is noticeable that, in general, r_c is of the order

² r_{200} is the radius where the density is 200 times the critical density of the universe, and defines the halo radius. In the CDM framework, concentrations are strongly correlated with the halo formation epoch, and must be in agreement with the N -body simulations.

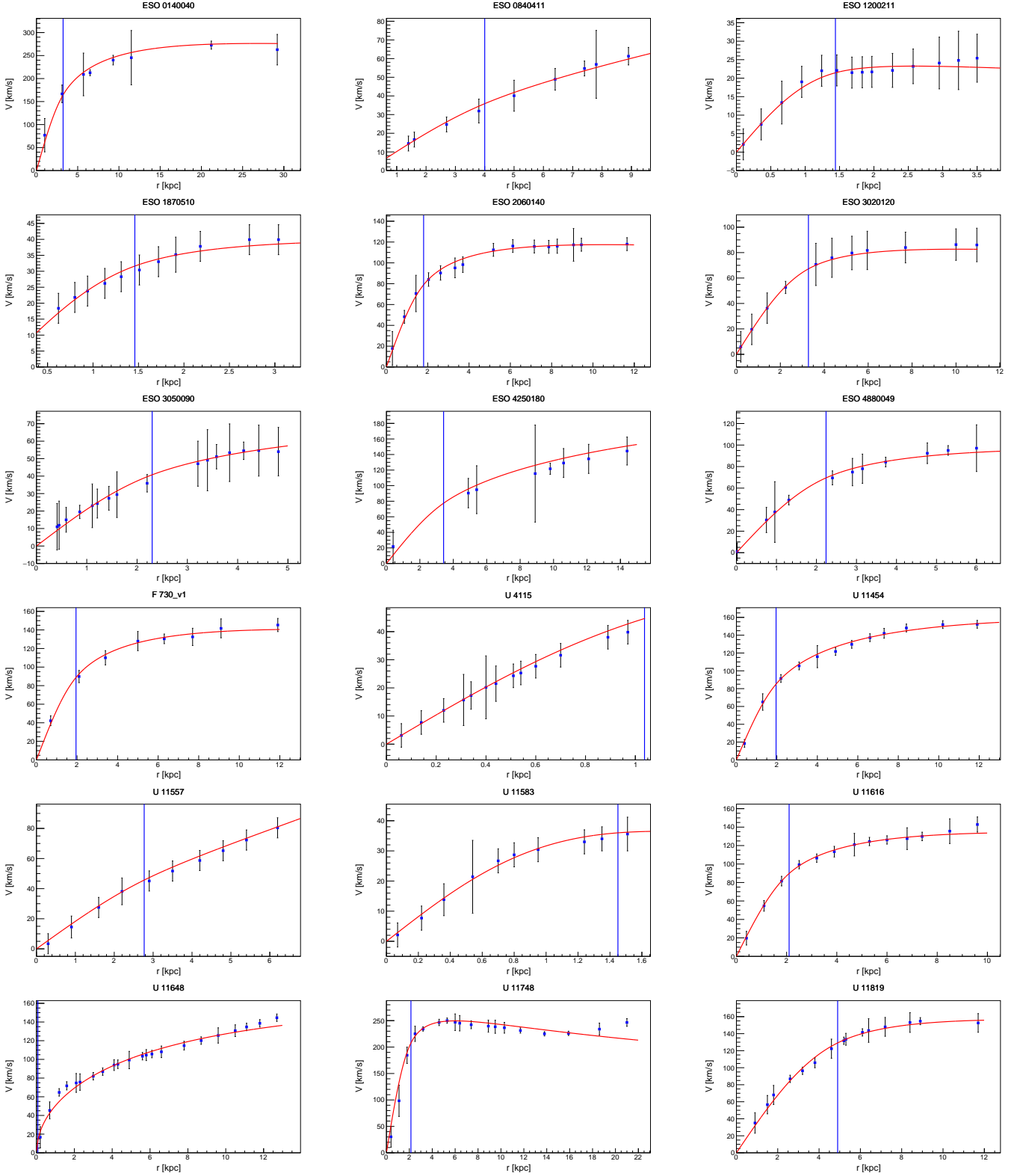


Figure 1. Best fits for the 18 high-resolution LSB galaxies without photometry for the ψ DM model using the soliton+NFW profile, corresponding to the fitting parameters shown in Table 3. The vertical lines correspond to the transition radii r_e . It is worth noting that in UGC11648 r_e is negligible, in this case the soliton-like contribution to the total profile is not relevant.

High-resolution LSB galaxies Soliton+NFW profile							
FITTING PARAMETERS							
Galaxy	$\rho_c (M_\odot/\text{pc}^3)$	r_c (kpc)	r_ϵ (kpc)	m_ψ (10^{-23} eV)	c	r_{200} (kpc)	χ^2_{red}
ESO-LV 014-0040	$0.222^{+0.044}_{-0.091}$	3.12 ± 0.76	3.23 ± 0.92	$0.352^{+0.063}_{-0.16}$	21.029	254.131	0.658
ESO-LV 084-0411	$0.00588^{+0.00068}_{-0.0015}$	$4.90^{+1.5}_{-0.99}$	$4.0^{+1.1}_{-1.6}$	$0.986^{+0.011}_{-0.58}$	—	—	0.092
ESO-LV 120-0211	$0.0266^{+0.0072}_{-0.0091}$	$1.01^{+0.17}_{-0.27}$	$1.44^{+0.35}_{-0.78}$	$9.6^{+1.6}_{-3.9}$	44.524	21.505	0.074
ESO-LV 187-0510	$0.0466^{+0.0092}_{-0.014}$	$1.20^{+0.27}_{-0.34}$	$1.46^{+0.36}_{-0.84}$	$5.28^{+0.87}_{-2.7}$	21.118	37.729	0.101
ESO-LV 206-0140	$0.172^{+0.031}_{-0.048}$	$1.65^{+0.31}_{-0.36}$	$1.80^{+0.39}_{-0.56}$	$1.34^{+0.25}_{-0.49}$	23.063	105.844	0.133
ESO-LV 302-0120	$0.0423^{+0.0068}_{-0.012}$	2.66 ± 0.57	$3.28^{+0.89}_{-1.4}$	$1.09^{+0.14}_{-0.48}$	21.556	78.971	0.032
ESO-LV 305-0090	$0.0265^{+0.0044}_{-0.0099}$	$2.26^{+0.68}_{-0.89}$	$2.30^{+0.77}_{-1.4}$	$2.589^{+0.020}_{-1.9}$	—	—	0.076
ESO-LV 425-0180	$0.0404^{+0.0067}_{-0.022}$	3.7 ± 1.1	$3.42^{+1.2}_{-0.83}$	$0.653^{+0.053}_{-0.35}$	6.139	251.269	0.509
ESO-LV 488-0490	$0.089^{+0.014}_{-0.025}$	1.98 ± 0.45	$2.24^{+0.52}_{-1.0}$	$1.37^{+0.22}_{-0.62}$	20.398	90.886	0.131
F730-V1	$0.181^{+0.035}_{-0.050}$	$1.84^{+0.34}_{-0.46}$	$1.95^{+0.39}_{-0.67}$	$1.08^{+0.22}_{-0.44}$	21.181	129.491	0.329
UGC 4115	$0.152^{+0.020}_{-0.043}$	$1.06^{+0.14}_{-0.66}$	$1.037^{+0.075}_{-0.79}$	$6.5^{+1.1}_{-5.8}$	14.418	91.143	0.132
UGC 11454	$0.157^{+0.030}_{-0.040}$	$1.96^{+0.39}_{-0.44}$	$1.96^{+0.44}_{-0.55}$	$1.0^{+0.21}_{-0.38}$	16.037	156.477	0.364
UGC 11557	$0.0191^{+0.0018}_{-0.0062}$	$3.7^{+1.4}_{-1.2}$	$2.77^{+0.94}_{-1.1}$	$1.152^{+0.072}_{-0.83}$	—	—	0.12
UGC 11583	$0.095^{+0.022}_{-0.026}$	$0.86^{+0.11}_{-0.26}$	$1.45^{+0.25}_{-1.0}$	$7.2^{+1.9}_{-3.0}$	—	—	0.097
UGC 11616	$0.163^{+0.019}_{-0.032}$	1.93 ± 0.28	$2.10^{+0.38}_{-0.49}$	$0.97^{+0.13}_{-0.27}$	22.378	122.007	0.189
UGC 11648	2.26 ± 0.25	$0.0858^{+0.010}_{-0.0093}$	$0.0737^{+0.0089}_{-0.0080}$	128^{+20}_{-30}	8.375	183.7	1.097
UGC 11748	$0.97^{+0.13}_{-0.23}$	$1.70^{+0.23}_{-0.21}$	2.14 ± 0.35	$0.502^{+0.056}_{-0.098}$	77.024	159.495	1.978
UGC 11819	$0.0710^{+0.0040}_{-0.0096}$	$3.92^{+0.51}_{-0.26}$	4.9 ± 1.1	$0.351^{+0.017}_{-0.077}$	27.976	139.349	0.28

Table 3. In this Table we show the resulting parameters ρ_c , r_c and r_ϵ for the ψ DM model with the soliton+NFW density profile (4), and the resulting boson mass m_ψ , all the quantities $\pm 1\sigma$ errors from the MCMC method used. We also show the resulting r_{200} from the NFW halo radius, concentration parameter c and χ^2_{red} errors for the 18 high-resolution LSB galaxies in de Blok et al. (2001a).

of the transition radius r_ϵ . This means that the soliton contribution is overlapped with the NFW halo (as we ask for a smooth transition between both profiles), and from the best fits, the values of r_ϵ do not correspond to $r_\epsilon > 3r_c$ (Schive et al. 014a).

Moreover, from Figure 1 it is easy to see that the soliton contribution to the total density profile is negligible for UGC11648, meanwhile for ESO4250180 and F730-V1 the soliton contribution spans only one observational point. For the last three galaxies the main contribution to the total velocity comes from the NFW profile, and for UGC11648 is not necessary to add the soliton part. Thus, to obtain the value of the boson mass we discarded the galaxy UGC11648, since from the negligible soliton contribution including m_ψ , the value obtained ($m_\psi \sim 10^{-21}$ eV) is not reliable. For the last 15 galaxies, the soliton contribution becomes important in order to fit the whole rotation curves. From the 17 galaxies (except from UGC11648) the values obtained for the boson mass are in the range $0.351 < m_\psi/10^{-23}\text{eV} < 9.6$, and core radius in $0.86 < r/\text{kpc} < 4.9$.

4.1.2 NGC galaxies with photometric data

In Table 4 we show the fitting parameters for the three representative galaxies in McGaugh et al. (2016) (NGC 7814, 6503, 3741) from the SPARC Database (Lelli et al. 2016b) and the three sample galaxies analysed in Robles & Matos (2013b) (NGC 1003, data from SPARC; NGC 1560, data from de Blok et al. (2001b); NGC 6946, data from McGaugh (2005)), for the ψ DM model with the soliton+NFW density profile (4). In the top panels we show the results for the galaxies without the photometric information and on the bottom panels the results including the bulge, disk and/or gas profiles, to analyse the effect of the baryons on the DM profile. We report the central density ρ_c and the core radius r_c , with the

resulting boson mass m_ψ , the transition radius r_ϵ and the reduced χ^2_{red} errors from the fitting method. The NFW parameters r_s and ρ_s were obtained from the last three fitting parameters, and we reported in the same Table the corresponding virial radii r_{200} and concentration parameters $c := r_{200}/r_s$.

In Figure 3 we show the plots for the corresponding fitting parameters presented in Table 4; the vertical lines show the corresponding transition radius r_ϵ for each galaxy. As we notice from Table 4 and Figure 3, the soliton+NFW profile fits the observations of NGC 7814, 6503 and 6946 only once the baryonic contribution is taken into account, except some points inside 5 kpc for NGC 6503. For NGC 1003 and NGC 6946, the transition radius r_ϵ is very small with respect to the maximum radius R_{max} , i.e. in these cases the whole rotation curve is better explained with the NFW profile and the soliton part does not introduce any improvement. For NGC 3741, which is a gas-dominated dwarf galaxy, the NFW profile fits the data very well, both with and without photometry. And for NGC1003 the fit is better including the baryons, but as we note, even when the fit is better, the NFW profile cannot explain the oscillations from the high-resolution observations (see also Robles & Matos 2013b); in this case the multistate SFDM profile is relevant (see Subsection 4.2). Finally, NGC 1560 is the only galaxy which remains with almost the same contribution from the ψ DM model, without and with the photometric information. The resulting ranges from the DM+baryons fits for the boson mass and core radius are: $0.264 < m_\psi/10^{-23}\text{eV} < 30.0$ and $0.311 < r/\text{kpc} < 4.84$, respectively.

4.2 Multistate SFDM fits

In this Subsection we present the results for the multistate SFDM model. It is worth mentioning that with a halo formed of one ex-

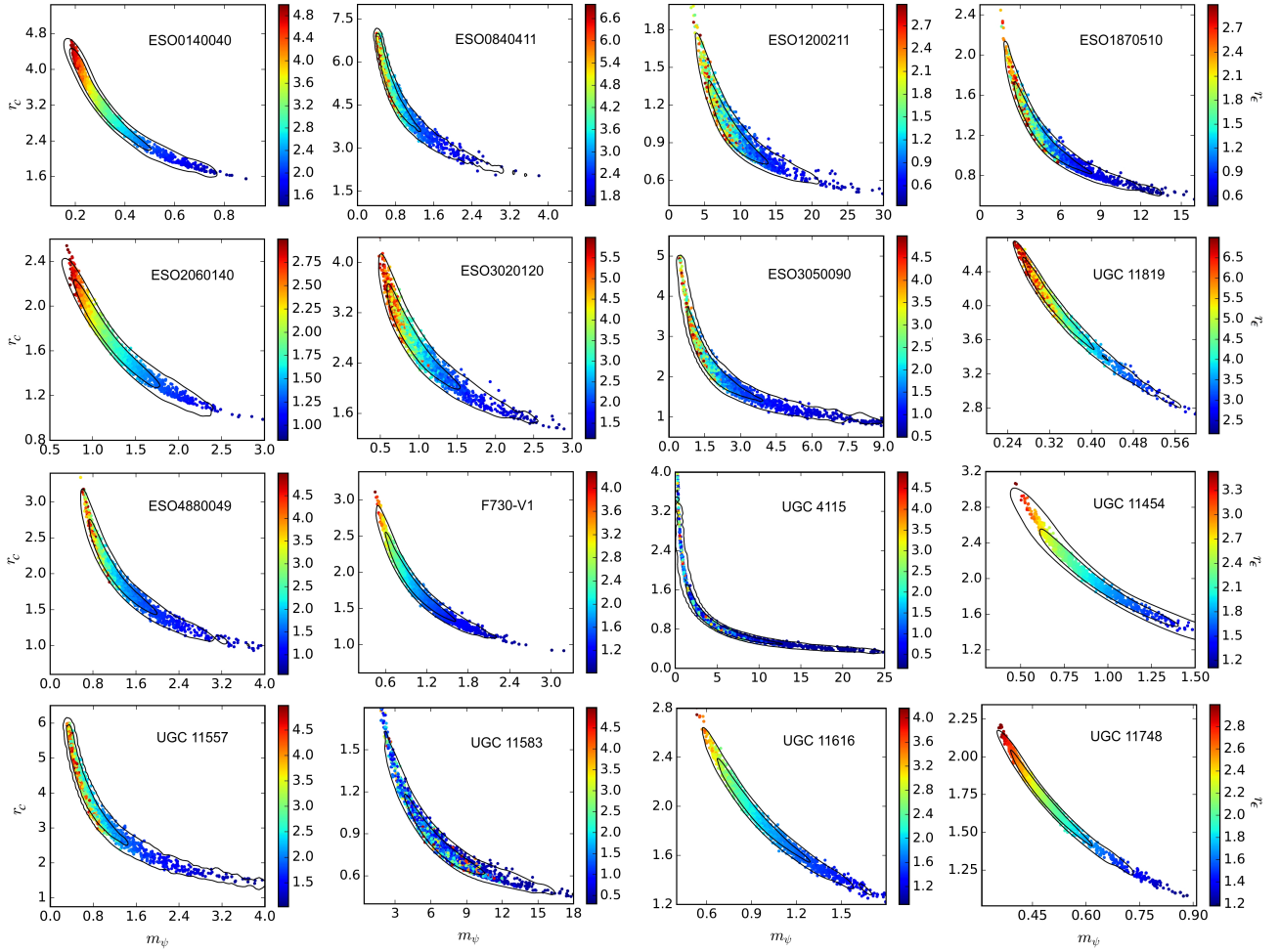


Figure 2. Posterior distributions for the parameters m_ψ (10^{-23} eV) and r_c (kpc), with the transition radius r_e (kpc) as the coloured scatter plot, for the high-resolution LSB galaxies in the ψ DM model, corresponding to the fitting parameters shown in Table 3. The contours are the 1σ and 2σ confidence regions. The plots were obtained with the GetDist 0.2.6 Package.

cited state only (two free parameters) it is possible to reproduce the rotation curves of some galaxies in the sample, however, in some cases, the number of the excited state is very high and as a result, the halo radius R is much greater than the maximum observable radius R_{max} ; in these cases, we preferred lower excitation states. Additionally, it is a well-known result that it is not possible to reproduce the whole rotation curve of big galaxies with the ground state only (Boehmer & Harko 2007; Robles & Matos 2012; Fernández-Hernández et al. 2016), so we do not include these results in the article.

The reported combinations of excited states are the ones that best reproduce the data. It is important to note that in some cases, the resulting configurations do not display the ground state as a dominant component. This might be the result of the different formation histories for every galaxy, including interactions with the baryonic matter resulting in diverse multistate configurations.

4.2.1 High-resolution LSB galaxies

In Table 5 we show the results for the 18 high-resolution LSB galaxies from de Blok et al. (2001a), for the multistate SFDM model (10) with two excited states. We report the fitting parameters: ρ_0^i and ρ_0^j (the central densities for the states i and j) and R

(the halo radius). We also computed the mass in the higher energy level M_j and in the lower state M_i , as well as the mass ratio $\eta = M_j/M_i$. Ureña-López & Bernal (2010) showed it is possible to have stable multistate configurations for values of $\eta = M_j/M_i \lesssim 1.3$ with respect to the ground state M_1 , i.e. the multistate haloes do not decay to the ground state. Therefore, from our results, we might argue that the final configurations are stable where the ground state appears as a dominant component. However, there are 8 galaxies in which the lower dominant state is $i=2, 3$ or even $i=6$; in these systems the final distribution in different excitation levels might be the final product of interactions with the baryonic matter. Further numerical simulations are needed to investigate the stability of multistate configurations without a dominant ground state and the influence of the baryonic matter in the SFDM halo.

With the haloes formed by two states only we found a very good agreement with the observational velocities for all the galaxies. Figure 4 shows the resulting best-fit profiles for these galaxies. For some galaxies, for example, F730-V1 and UGC 11748, the fits might be improved by introducing a third excited state; however it is not necessary to include additional degrees of freedom and we do not report these fits in the work.

NGC galaxies with photometric data

DM-only fits Soliton+NFW profile							
Galaxy	ρ_c (M_\odot/pc^3)	r_c (kpc)	r_ϵ (kpc)	m_ψ (10^{-23}eV)	c	r_{200} (kpc)	χ^2_{red}
NGC7814	47.3 ± 4.8	$0.0872^{+0.010}_{-0.0067}$	$0.0774^{+0.0096}_{-0.0063}$	$27.0^{+2.8}_{-5.5}$	69.425	147.32	5.541
NGC6503	$14.3^{+1.9}_{-1.3}$	$0.0464^{+0.0036}_{-0.0028}$	$0.0402^{+0.0032}_{-0.0025}$	171 ± 20	28.59	98.725	6.38
NGC3741	$1.33^{+0.13}_{-0.20}$	0.0367 ± 0.0050	0.0315 ± 0.0043	932^{+200}_{-300}	6.032	72.329	0.646
NGC1003	$0.90^{+0.52}_{-0.24}$	$0.154^{+0.046}_{-0.065}$	$0.133^{+0.040}_{-0.056}$	69^{+70}_{-30}	8.778	124.246	4.864
NGC1560	$0.0563^{+0.0064}_{-0.0088}$	1.39 ± 0.18	1.31 ± 0.20	$3.16^{+0.50}_{-0.78}$	7.983	95.974	0.395
NGC6946	$0.0514^{+0.0032}_{-0.0047}$	$4.92^{+0.36}_{-0.30}$	6.28 ± 0.70	$0.254^{+0.019}_{-0.029}$	27.294	150.211	1.616

DM+baryons fits Soliton+NFW profile							
Galaxy	ρ_c (M_\odot/pc^3)	r_c (kpc)	r_ϵ (kpc)	m_ψ (10^{-23}eV)	c	r_{200} (kpc)	χ^2_{red}
NGC7814	$0.0557^{+0.0066}_{-0.014}$	$4.84^{+0.80}_{-0.66}$	5.6 ± 1.2	$0.264^{+0.028}_{-0.070}$	18.492	177.278	0.86
NGC6503	$0.0459^{+0.0041}_{-0.0068}$	$2.81^{+0.29}_{-0.24}$	$3.07^{+0.38}_{-0.34}$	$0.831^{+0.072}_{-0.13}$	13.809	106.975	1.547
NGC3741	$0.0633^{+0.0082}_{-0.029}$	$0.68^{+0.21}_{-0.27}$	$0.60^{+0.18}_{-0.25}$	$18.0^{+1.4}_{-12}$	4.687	93.217	2.115
NGC1003	$0.231^{+0.061}_{-0.032}$	$0.311^{+0.033}_{-0.052}$	$0.269^{+0.029}_{-0.045}$	30.0^{+8}_{-4}	5.062	135.755	2.93
NGC1560	$0.0411^{+0.0042}_{-0.0065}$	1.46 ± 0.20	$1.38^{+0.20}_{-0.23}$	$3.35^{+0.47}_{-0.83}$	7.113	86.89	0.234
NGC6946	$0.27^{+0.16}_{-0.12}$	$0.62^{+0.33}_{-0.27}$	$0.55^{+0.30}_{-0.24}$	$8.7^{+7.9}_{-4.9}$	9.376	143.84	5.34

Table 4. In this Table we show the fitting parameters ρ_c , r_c and r_ϵ , the resulting boson mass m_ψ , the concentration parameters c and r_{200} radii from the NFW profile, and the χ^2_{red} errors for the soliton+NFW profile, for the NGC galaxies with photometric information. In the top panel we show the DM-only fits and in the bottom panel the fits taking into account the baryonic contribution.

High-resolution LSB galaxies

Multistate SFDM with two states

FITTING PARAMETERS								
Galaxy	i,j	R (kpc)	ρ_0^i (M_\odot/pc^3)	ρ_0^j (M_\odot/pc^3)	M_i ($10^{10} M_\odot$)	M_j ($10^{10} M_\odot$)	η	χ^2_{red}
ESO-LV 014-0040	2,7	46.93 ± 2.071	0.031 ± 0.0052	0.2 ± 0.025	26.5219	15.6727	0.59	0.1262
ESO-LV 084-0411	1,6	19.7 ± 8.85	0.0039 ± 0.0012	0.0033 ± 0.0024	0.7595	0.0214	0.03	0.0029
ESO-LV 120-0211	3,8	15.56 ± 2.919	0.0035 ± 0.0024	0.029 ± 0.0098	0.0253	0.0264	1.04	0.0204
ESO-LV 187-0510	2,7	8.404 ± 1.512	0.024 ± 0.0078	0.045 ± 0.022	0.1014	0.0127	0.13	0.0029
ESO-LV 206-0140	2,7	23.1 ± 1.51	0.021 ± 0.0037	0.17 ± 0.02	2.0117	1.4056	0.70	0.2341
ESO-LV 302-0120	1,2	12.02 ± 2.235	0.0097 ± 0.0078	0.028 ± 0.0086	1.0633	0.771	0.73	0.0084
ESO-LV 305-0090	1,5	7.699 ± 1.987	0.016 ± 0.0048	0.025 ± 0.013	0.3412	0.0173	0.051	0.0078
ESO-LV 425-0180	1,9	26.3 ± 5.25	0.008 ± 0.0026	0.19 ± 0.099	5.4805	1.5405	0.28	0.0054
ESO-LV 488-0490	3,8	23.8 ± 2.954	0.035 ± 0.0094	0.064 ± 0.017	1.0278	0.2134	0.21	0.0054
F730-V1	1,4	14.8 ± 1.235	0.02 ± 0.0041	0.18 ± 0.02	3.9812	1.7529	0.44	1.0227
UGC 4115	1,5	2.25 ± 0.978	0.13 ± 0.037	0.031 ± 0.086	0.0356	0.0004	0.011	0.0023
UGC 11454	1,3	14.27 ± 0.624	0.025 ± 0.0026	0.1 ± 0.0077	4.4521	1.7955	0.40	0.2939
UGC 11557	1,5	23.31 ± 14.06	0.01 ± 0.0028	0.0079 ± 0.0049	0.8712	0.0603	0.069	0.0392
UGC 11583	1,4	6.413 ± 2.922	0.015 ± 0.031	0.087 ± 0.024	0.0199	0.0227	1.14	0.0801
UGC 11616	2,5	25.56 ± 1.844	0.021 ± 0.0041	0.11 ± 0.0078	2.5003	1.7909	0.72	0.5551
UGC 11648	1,7	19.36 ± 1.131	0.012 ± 0.0012	0.23 ± 0.017	4.3513	1.4266	0.33	0.6469
UGC 11748	6,9	41.12 ± 0.8	0.27 ± 0.032	0.33 ± 0.051	16.8126	9.5328	0.57	1.6754
UGC 11819	2,7	24.7 ± 0.997	0.043 ± 0.0034	0.062 ± 0.013	5.2072	0.5528	0.11	0.0931

Table 5. In this Table we show the fitting parameters R , ρ_0^i and ρ_0^j for two excitation states i, j in the multistate SFDM model, for the 18 high-resolution LSB galaxies in [de Blok et al. \(2001a\)](#). We report the resulting masses M_i and M_j for each state, the mass ratio $\eta = M_j/M_i$ and χ^2_{red} errors from the fitting method.

4.2.2 NGC galaxies with photometric data

In Table 6 we present the results for the multistate SFDM model, for the three representative SPARC galaxies in [McGaugh et al. \(2016\)](#) (NGC 7814, 6503, 3741) and the three sample galaxies analysed in [Robles & Matos \(2013b\)](#) (NGC 1003, data from SPARC;

NGC 1560, data from [de Blok et al. \(2001b\)](#); NGC 6946, data from [McGaugh \(2005\)](#)). For the haloes formed by two states we report: ρ_0^i , ρ_0^j and R , all $\pm 1\sigma$ errors from the fitting method used. We also report the total masses M_i and M_j , and the resulting mass ratios $\eta = M_j/M_i$. For the DM+baryons fits we obtain four galaxies with a dominant ground state and two with excited states only. In

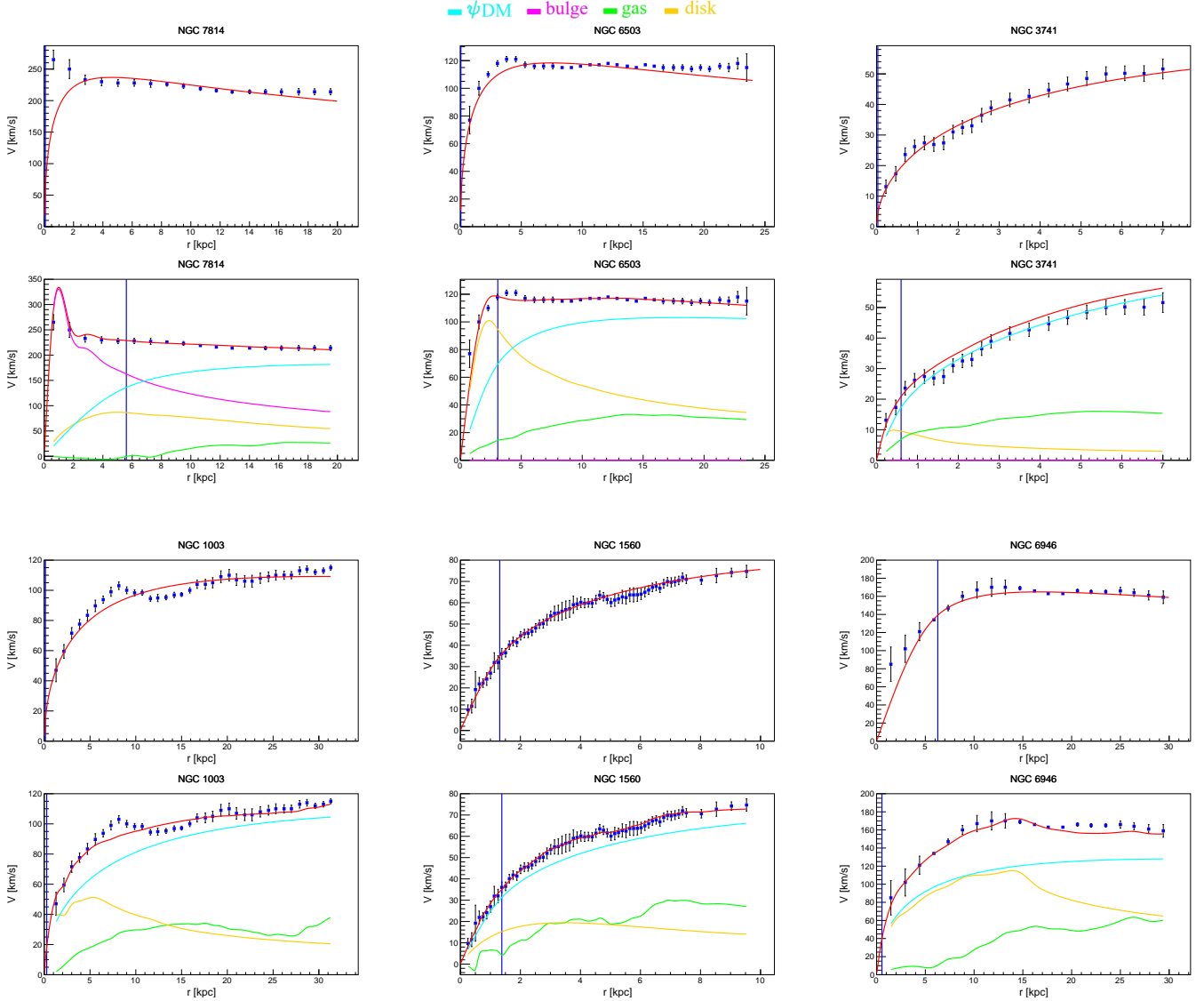


Figure 3. Best fits in the ψ DM model for the soliton+NFW profile for the NGC galaxies with photometric data. The fitting parameters are shown in Table 4. We compare the results without and taking into account the baryonic information. The vertical lines are the corresponding transition radii r_ϵ from the MCMC method.

the case of the galaxies with $i = 1$ the values of the mass ratios are $\eta \lesssim 1.3$, consistent with the stability condition mentioned in Subsection 4.2.1. The η values for the DM-only fits are not reliable.

Figure 5 shows the resulting profiles with these fitting parameters, without and taking into account the baryonic information. For NGC 7814, the bulge-dominated galaxy, once the photometric information is included, the model reproduces very well the observations. For NGC 6503, the disk-dominated galaxy, the best fit fails at reproducing some regions, even taking into account the baryonic information. For NGC 3741, the gas-dominated galaxy, and for NGC 1560, the fits (without and with photometry) are very good. For NGC 1003 and 6946 the inner regions are reproduced once the baryonic information is included. For NGC 1003 the multistate model reproduces very well the wiggles, which are not reproduced by the baryonic components (see the previous results by Robles & Matos 2013b), and as mentioned in Subsection 4.1.2, in this case the NFW profile is not capable to reproduce the oscillations.

For NGC 6503 we present the three states configuration (four fitting parameters) in Table 6 and the resulting profile in Figure 6. For the other galaxies the fittings might be improved by introducing a third excited state, but is not necessary to introduce more degrees of freedom since two excited states are well enough. It is worth noting that in these cases the other intermediate states (including the ground state) might be present in the SFDM halo, but their contribution to the total density profile is negligible with respect to the dominant ones.

5 DISCUSSION AND CONCLUSIONS

From the ψ DM simulations it is found that the haloes are formed by prominent dense cores which approximate well the soliton-like solutions of the Schrödinger-Poisson equation with a sharp transition to the NFW profile (Schive et al. 014a,b). In the present work we impose not only a continuity condition between both profiles,

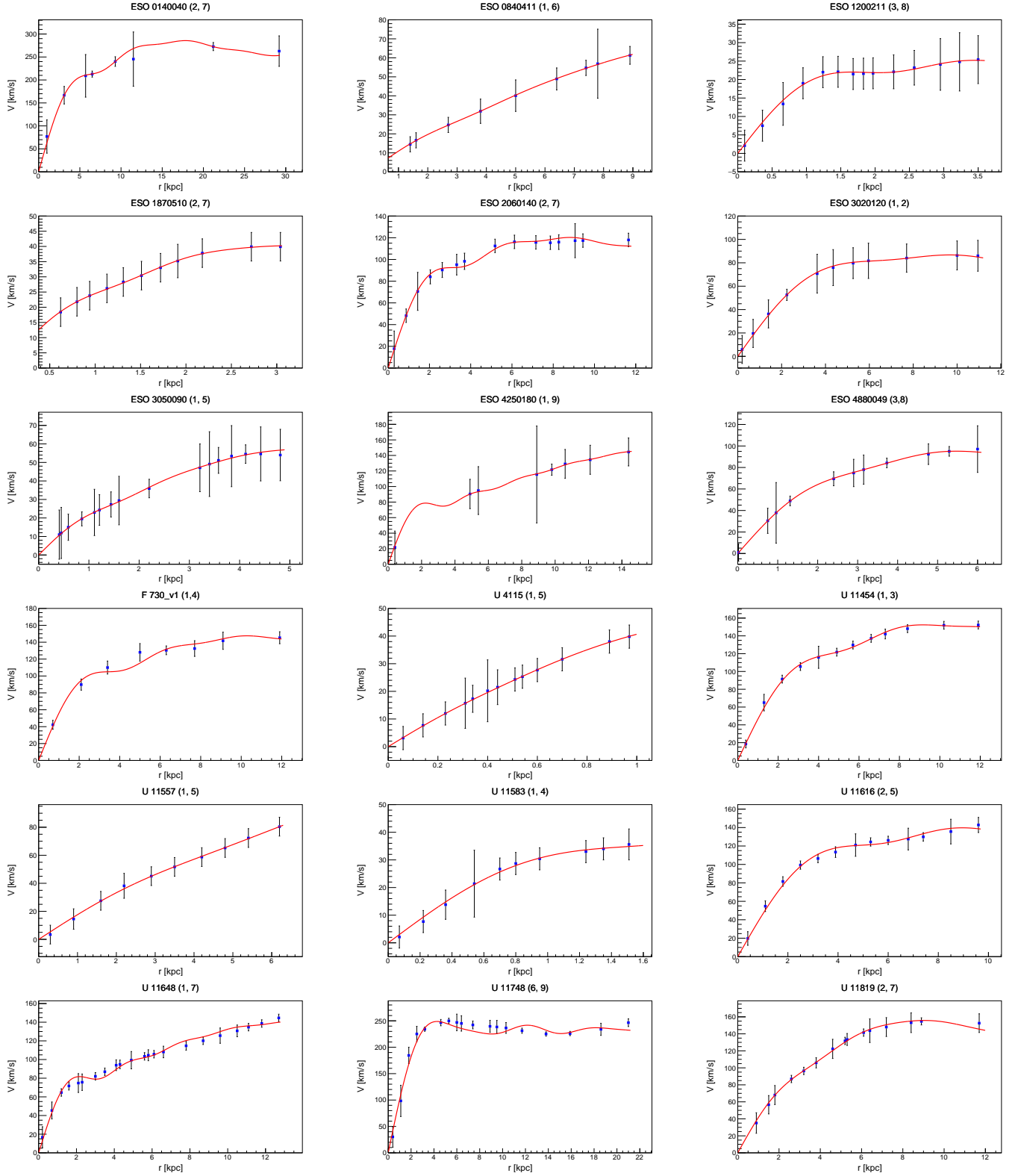


Figure 4. Best-fit profiles for the 18 high-resolution LSB galaxies in the multistate SFDM model with two excited states (i, j) . The corresponding fitting parameters are shown in Table 5.

NGC galaxies with photometric data

DM-only fits									
Multistate SFDM with two states									
Galaxy	i,j	$R(kpc)$	$\rho_0^i (\text{M}_\odot/\text{pc}^3)$	$\rho_0^j (\text{M}_\odot/\text{pc}^3)$	$M_i (10^{10} \text{M}_\odot)$	$M_j (10^{10} \text{M}_\odot)$	η	χ^2_{red}	
NGC7814	1,9	16.13 ± 0.1782	$1.85 \times 10^{-8} \pm 0.00011$	5.51 ± 0.1325	5.23×10^{-6}	22.2066	4.25×10^6	6.55	
NGC6503	3,9	20.25 ± 0.22	0.034 ± 0.0034	0.67 ± 0.03	2.2839	5.0818	2.23	2.05	
NGC3741	1,7	8.825 ± 0.42	0.0079 ± 0.00069	0.11 ± 0.00896	0.3277	0.0785	0.24	0.31	
NGC1003	1,4	43.36 ± 0.423	$0.0007 \pm 3.21 \times 10^{-5}$	0.025 ± 0.00055	3.2796	5.9964	1.83	1.46	
NGC1560	1,3	13.93 ± 0.305	0.0057 ± 0.00026	0.031 ± 0.0009	0.8117	0.3946	0.49	0.61	
NGC6946	2,3	42.12 ± 0.607	0.0091 ± 0.0008	0.029 ± 0.0008	7.0211	10.414	1.48	1.39	
DM+baryons fits									
Multistate SFDM with two states									
NGC7814	4,9	102.6 ± 4.968	0.0089 ± 0.0010	0.039 ± 0.00326	8.818	6.902	0.78	0.388	
NGC6503	2,7	44.23 ± 0.607	0.0032 ± 0.000165	0.053 ± 0.0014	2.194	3.270	1.49	4.05	
NGC3741	1,6	8.84 ± 0.43	0.0073 ± 0.00066	0.059 ± 0.00597	0.306	0.059	0.19	0.21	
NGC1003	1,4	44.69 ± 0.72	$0.0009 \pm 3.6 \times 10^{-5}$	0.015 ± 0.0005	4.425	3.920	0.89	0.525	
NGC1560	1,3	14.78 ± 0.412	0.004 ± 0.00023	0.022 ± 0.00085	0.657	0.339	0.52	0.486	
NGC6946	1,3	38.10 ± 0.676	0.002 ± 0.0001	0.020 ± 0.00055	6.559	5.752	0.88	0.37	
DM+baryons fit									
Multistate SFDM with three states									
Galaxy	i,j,k	R (kpc)	ρ_0^i ($\text{M}_\odot/\text{pc}^3$)	ρ_0^j ($\text{M}_\odot/\text{pc}^3$)	ρ_0^k ($\text{M}_\odot/\text{pc}^3$)	M_i (10^{10}M_\odot)	M_j (10^{10}M_\odot)	M_k (10^{10}M_\odot)	χ^2_{red}
NGC6503	2,4,7	49.31 ± 2.06	0.0021 ± 0.00031	0.0068 ± 0.00056	0.029 ± 0.0021	1.9619	1.6204	2.074	1.51

Table 6. In this Table we show the fitting parameters R , ρ_0^i and ρ_0^j for two excitation states i, j in the multistate SFDM model, for the NGC galaxies with photometric data. We report the resulting masses M_i and M_j for each state, the mass ratio $\eta = M_j/M_i$ and χ_{red}^2 errors from the fitting method. In the top panel we show the DM-only fits and in the middle one the fits taking into account the baryonic contribution. In the bottom panel are the fitting parameters for NGC 6503 with three excited states.

but also the differentiability in the transition between the soliton and the NFW functions, as a convenient restriction to deal with three free parameters only (Appendix A). As a consequence of this additional restriction, we obtain transition radii $r_\epsilon \gtrsim r_c$ compared to the core radii, which is different from the expected $r_\epsilon > 3r_c$ in the simulations (Schive et al. 014a). In our case, the transition occurs before to have a smoother function.

In Figure 7 we show the resulting distribution of core radii r_c vs. boson masses m_ψ for the 17 LSB galaxies (except for UGC11648 with a negligible soliton-contribution); and for the NGC galaxies with baryonic information included for the soliton+NFW density profile in the ψ DM model. For these galaxies, we found that the resulting m_ψ is in the range $0.351 < m_\psi/10^{-23} \text{eV} < 9.6$ and core radius in $0.86 < r_c/\text{kpc} < 4.90$ from the LSB galaxies (Table 3); and masses in $0.264 < m_\psi/10^{-23} \text{eV} < 30.0$ and core radius in $0.311 < r_c/\text{kpc} < 4.84$ from the NGC galaxies with baryonic data (Table 4). Remarkably, there is a large scattering in the distribution of the boson mass m_ψ and the core radius r_c , since the rotation curves of the galaxies span a wide range in sizes ($R_{\text{max}} \sim 1 - 30$ kpc). From the Jeans analysis of dwarf spheroidal galaxies ($r_{\text{max}} \sim 0.5 - 2$ kpc), Chen et al. (2016) found $8.1 < m_\psi/10^{-23} \text{eV} < 62$ and $0.2 < r_c/\text{kpc} < 1$, and from a detailed analysis by González-Morales et al. (2016) using kinematic mock data of Fornax and Sculptor, the constraint is $m_\psi < 4 \times 10^{-23} \text{eV}$. Our results are overlapped with these two ranges.

It is important to note that a strong cosmological constraint on the boson mass from damped Lyman- α observations is $m_\psi >$

10^{-23}eV (Sarkar et al. 2016). In this work we do not impose such restriction and found 6 LSB galaxies and 2 NGC+baryons galaxies in the range $m_\psi < 10^{-23} \text{eV}$. As it is known, in the SFDM there is a sharp break in the matter power spectrum leading to a natural suppression of substructure below a scale depending on the boson mass: $k \sim m_\psi^{1/3}$. The cosmological implications for such light boson masses would imply lesser substructure than observed. For these galaxies, we expect that the range in core radius will decrease as the boson mass increases to have $m_\psi > 10^{-23} \text{eV}$, once the cosmological restriction is imposed, as the trend shown in Figure 7.

For the exact multistate SFDM, which includes a self-interaction and multistate solutions coming from thermal excitations, we find that the model is consistent with the rotation curves for both LSB and NGC galaxies with photometric information. For combinations of two excited states (three free parameters), the χ_{red}^2 errors are, in general, smaller for the multistate SFDM profile compared to the soliton+NFW fits, except for 3 of the 18 LSB galaxies, and for 2 of the 6 NGC galaxies with photometric data, where only for NGC 6503 the error is significant and we fit the data with three excited states. This is important since the number of free parameters in every model is the same: three for the soliton+NFW profile with the differentiability condition and three for the multistate SFDM model with two excited states. In this sense, the multistate SFDM model fits the observations in a simpler way than the soliton+NFW profile.

For the resulting two-states configurations in the multistate SFDM model, we assume the stability threshold by Ureña-López & Bernal (2010), where for multistate systems where the mass ra-

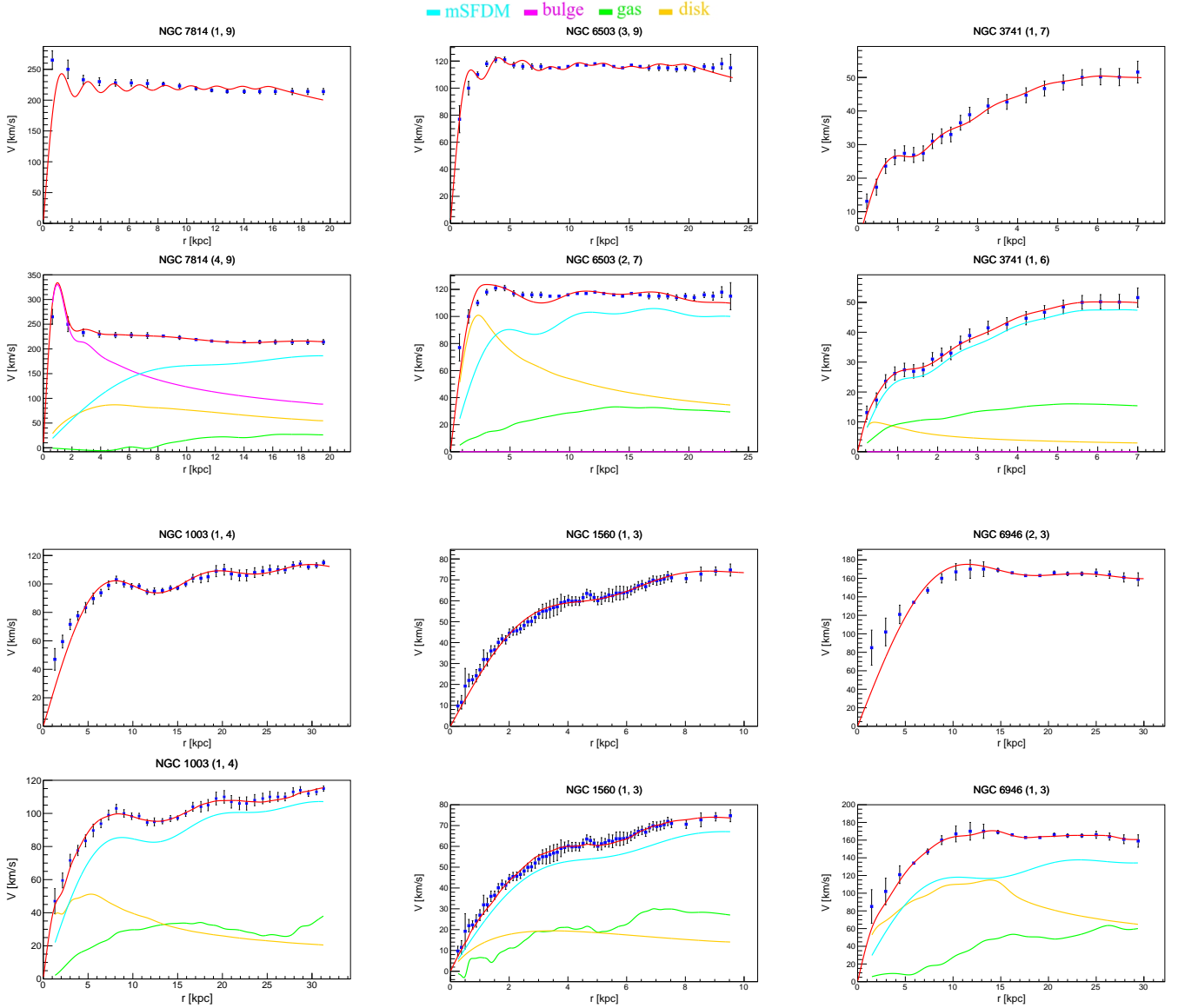


Figure 5. Best fits for the NGC galaxies with photometric data in the multistate SFDM model with two excited states (i, j) , for DM-only and DM+baryons contribution. The corresponding fitting parameters are shown in Table 6.

tions $\eta = M_j/M_1 \lesssim 1.3$, with respect to the ground state M_1 , the excited state j does not decay to the ground state, i.e. is a stable multistate configuration. In our fits, we obtained 10 of 18 LSB galaxies and 4 of 6 NGC galaxies with baryonic contribution with a dominant ground state $j=1$; for these galaxies we argue that they might be stable systems since the mass ratios satisfy such restriction. For the galaxies with excited states only, the final distribution in different excitation levels might be the final product of interactions with the baryonic matter. Further numerical simulations including the baryonic components are needed to investigate the stability of the multistate configurations and the influence of the baryonic matter in the SFDM halo.

Figure 8 shows the resulting soliton+NFW and multistate SFDM density profiles for three sample LSB galaxies. There is an evident overlap between both profiles, showing the core-like behaviour at the innermost radii, the oscillations at intermediate radii (inherent in the multistate SFDM model), and a steeper slope of

the multistate SFDM with respect to the NFW decline at the outermost radii, defining more compact SFDM haloes. Such overlap was discussed in Bernal et al. (2016) from the results of fitting the multistate SFDM model and the NFW profile to the X-ray observations of clusters of galaxies. Even when, at this point, with the multistate SFDM model it is not possible to constrain the boson properties, m_ψ and λ , we show that this model is a theoretically motivated framework for realistic SFDM haloes, fitting in a simple way the observations. Moreover, as discussed by Bernal et al. (2016), the analytic multistate solution is an interesting alternative which can be used as a fitting-function for several astrophysical systems, along with or as an alternative to the empirical soliton+NFW profile.

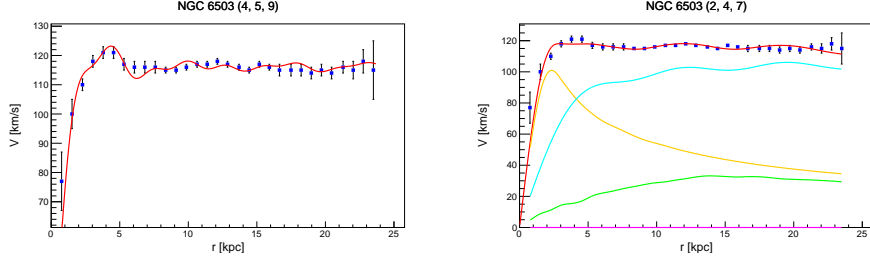


Figure 6. The same as Fig. 5 for NGC 6503 with three excited states (i, j, k) .

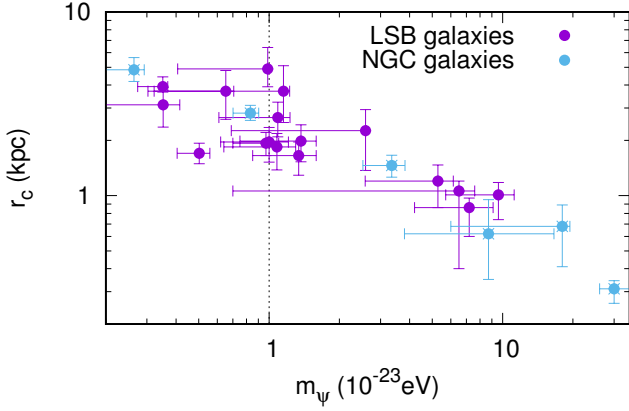


Figure 7. Distribution of resulting core radii r_c vs. boson masses m_ψ from the soliton+NFW density profile in the ψ DM model, for 17 LSB and 6 NGC (including baryonic information) galaxies, $\pm 1\sigma$ errors from the MCMC method. The vertical line at $m_\psi = 10^{-23}$ eV shows the cosmological constraint by Lyman- α observations (Sarkar et al. 2016).

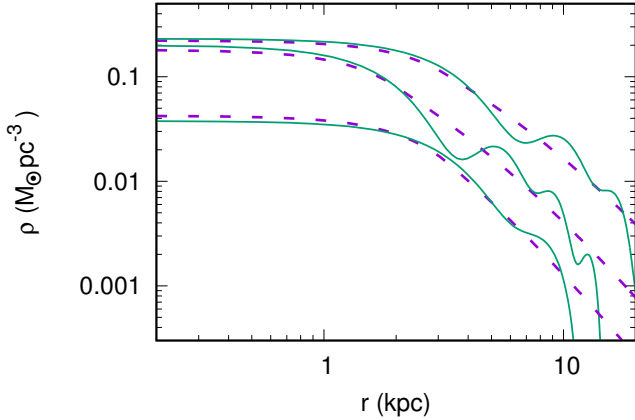


Figure 8. Resulting density profiles for three sample LSB galaxies. The dashed lines show the soliton+NFW profiles and the solid lines the corresponding multistate SFDM fits. The overlap between both profiles is evident for the galaxies, showing the core-like behaviour at the innermost radii, the oscillations around the NFW-region inherent in the multistate profile and the steeper slope at the outermost radii of the multistate SFDM model compared to the NFW profile. Every galaxy shows different oscillations depending on its particular multistate combination.

6 ACKNOWLEDGEMENTS

We gratefully acknowledge Stacy McGaugh for providing us the observational data used in this article and for helpful comments and discussions about his work in previous publications. We thank Luis Arturo Ureña-López who provided insights and suggestions for the final results in this article. This work was partially supported by CONACyT México under grants CB-2011 No. 166212, CB-2014-01 No. 240512, Project No. 269652 and Fronteras Project 281; Xihuatlan and Abacus clusters at Cinvestav, IPN; I0101/131/07 C-234/07 of the Instituto Avanzado de Cosmología (IAC) collaboration (<http://www.iac.edu.mx>).

APPENDIX A: SOLITON+NFW MASS PROFILE

We restricted the total soliton+NFW density profile (4) in the ψ DM model to be continuous and differentiable at the transition radius r_ϵ :

$$\rho_{\text{sol}}(r_\epsilon) = \rho_{\text{NFW}}(r_\epsilon), \quad (\text{A1})$$

$$\rho'_{\text{sol}}(r_\epsilon) = \rho'_{\text{NFW}}(r_\epsilon). \quad (\text{A2})$$

With these restrictions the two NFW parameters r_s and ρ_s can be written in terms of the other three free parameters, ρ_c , r_c and r_ϵ as:

$$r_s(r_c, r_\epsilon) = \left(\frac{b-3}{1-b} \right) r_\epsilon \quad (\text{A3})$$

$$\rho_s(\rho_c, r_c, r_\epsilon) = \frac{1-b}{(b-3)^3} \frac{4\rho_c}{[1 + 0.091(r_\epsilon/r_c)^2]^8}, \quad (\text{A4})$$

where $b := 1.456(r_\epsilon/r_c)^2/[1 + 0.091(r_\epsilon/r_c)^2]$ and $\rho_c := 1.9(m_\psi/10^{-23}\text{eV})^{-2}(r_c/\text{kpc})^{-4}$.

The total soliton+NFW mass is given by

$$M_{\psi\text{DM}}(r) = \begin{cases} M_{\text{sol}}(r), & \text{if } r \leq r_\epsilon; \\ M_{\text{sol}}(r_\epsilon) - M_{\text{NFW}}(r_\epsilon) + M_{\text{NFW}}(r), & \text{if } r > r_\epsilon; \end{cases} \quad (\text{A5})$$

where the core mass function is given by (Chen et al. 2016)

$$M_{\text{sol}}(r) = \frac{4.2 \times 10^6 M_\odot}{(m_\psi/10^{-23}\text{eV})^2 (r_c/\text{kpc})} \frac{1}{(1+a^2)^7} [3465a^{13} + 23100a^{11} + 65373a^9 + 101376a^7 + 92323a^5 + 48580a^3 - 3465a + 3465(1+a^2)^7 \arctan a], \quad (\text{A6})$$

with $a := 0.301(r/r_c)$, and the NFW mass profile given by (Navarro et al. 1997)

$$M_{\text{NFW}}(r) = 4\pi\rho_s r_s^3 \left[\ln \left(1 + \frac{r}{r_s} \right) - \frac{r/r_s}{1 + r/r_s} \right]. \quad (\text{A7})$$

References

- Alcubierre M., Guzman F. S., Matos T., Nunez D., Ureña-López L. A., Wiederhold P., 2002, *Class. Quant. Grav.*, 19, 5017
- Arbey A., Lesgourgues J., Salati P., 2001, *Phys. Rev. D*, 64, 123528
- Arbey A., Lesgourgues J., Salati P., 2002, *Phys. Rev.*, D65, 083514
- Baldeschi M. R., Ruffini R., Gelmini G. B., 1983, *Phys. Lett.*, B122, 221
- Bennett C. L., et al., 2013, *The Astrophysical Journal Supplement Series*, 208, 20
- Bernal A., Matos T., Nunez D., 2008, *Rev. Mex. A.A.*, 44 No. 1, 149
- Bernal A., Barranco J., Alic D., Palenzuela C., 2010, *Phys. Rev. D*, 81, 044031
- Bernal T., Robles V. H., Matos T., 2016, preprint, ([arXiv:1609.08644](https://arxiv.org/abs/1609.08644))
- Bertone G., Hooper D., Silk J., 2005, *Phys. Rep.*, 405, 279
- Boehmer C. G., Harko T., 2007, *JCAP*, 0706, 025
- Boylan-Kolchin M., Bullock J. S., Kaplinghat M., 2011, *MNRAS*, 415, L40
- Bray H. L., 2010, preprint, ([arXiv:1004.4016](https://arxiv.org/abs/1004.4016))
- Bray H. L., 2012, preprint, ([arXiv:1212.5745](https://arxiv.org/abs/1212.5745))
- Brun R., Rademakers F., 1997, *Nuclear Instruments and Methods in Physics Research A*, 389, 81
- Burkert A., 1996, *IAU Symp.*, 171, 175
- Calabrese E., Spergel D. N., 2016, *MNRAS*, 460, 4397
- Caputi K. I., et al., 2015, *Astrophys. J.*, 810, 73
- Chen S.-R., Schive H.-Y., Chiueh T., 2016, preprint, ([arXiv:1606.09030](https://arxiv.org/abs/1606.09030))
- Davé R., Spergel D. N., Steinhardt P. J., Wandelt B. D., 2001, *ApJ*, 547, 574
- Di Cintio A., Brook C. B., Macciò A. V., Stinson G. S., Knebe A., Dutton A. A., Wadsley J., 2014, *MNRAS*, 437, 415
- Díez-Tejedor A., Gonzalez-Morales A. X., Profumo S., 2014, *Phys. Rev.*, D90, 043517
- Dutta P., Begum A., Bharadwaj S., Chengalur J. N., 2009, *MNRAS*, 398, 887
- Elbert O. D., Bullock J. S., Garrison-Kimmel S., Rocha M., Oñorbe J., Peter A. H. G., 2015, *MNRAS*, 453, 29
- Fernández-Hernández L., Rodríguez-Meza M., Matos T., 2016, In preparation
- Gamerman D., 1997, *Markov Chain Monte Carlo: Stochastic Simulation for Bayesian Inference*. Chapman & Hall/CRC Texts in Statistical Science, Taylor & Francis
- Gelman A., Rubin D. B., 1992, *Statistical Science*, 7, 457
- Gentile G., Salucci P., Klein U., Granato G. L., 2007a, *MNRAS*, 375, 199
- Gentile G., Famaey B., Combes F., Kroupa P., Zhao H. S., Tíret O., 2007b, *Astron. Astrophys.*, 472, L25
- González-Morales A. X., Marsh D. J. E., Peñarrubia J., Ureña-López L., 2016, preprint, ([arXiv:1609.05856](https://arxiv.org/abs/1609.05856))
- Goodman J., 2000, *New Astron.*, 5, 103
- Governato F., et al., 2010, *Nature*, 463, 203
- Guzman F. S., Matos T., Villegas H. B., 1999, *Astron. Nachr.*, 320, 97
- Harko T., 2011, *JCAP*, 1105, 022
- Hlozek R., Grin D., Marsh D. J. E., Ferreira P. G., 2015, *Phys. Rev.*, D91, 103512
- Hu W., Barkana R., Gruzinov A., 2000, *Physical Review Letters*, 85, 1158
- Hui L., Ostriker J. P., Tremaine S., Witten E., 2016, preprint, ([arXiv:1610.08297](https://arxiv.org/abs/1610.08297))
- Ibata R. A., et al., 2013, *Nature*, 493, 62
- Ibata N. G., Ibata R. A., Famaey B., Lewis G. F., 2014, *Nature*, 511, 563
- Ji S. U., Sin S. J., 1994, *Phys. Rev. D*, 50, 3655
- Klypin A., Kravtsov A. V., Valenzuela O., Prada F., 1999, *ApJ*, 522, 82
- Koda J., et al., 2015, *ApJ*, 802, L24
- Kolb E., Turner M., 1994, *The Early Universe*. Frontiers in physics, Westview Press
- Kroupa P., 2012, *Publ. Astron. Soc. Austral.*, 29, 395
- Kroupa P., et al., 2010, *A&A*, 523, A32
- Lee J.-w., Koh I.-g., 1996, *Phys. Rev.*, D53, 2236
- Lelli F., McGaugh S. S., Schombert J. M., Pawłowski M. S., 2016a, preprint, ([arXiv:1610.08981](https://arxiv.org/abs/1610.08981))
- Lelli F., McGaugh S. S., Schombert J. M., 2016b, *AJ*, 152, 157
- Li B., Rindler-Daller T., Shapiro P. R., 2014, *Phys. Rev. D*, 89, 083536
- Lora V., Magaña J., 2014, *J. Cosmology Astropart. Phys.*, 9, 011
- Lora V., Magaña J., Bernal A., Sánchez-Salcedo F. J., Grebel E. K., 2012, *J. Cosmology Astropart. Phys.*, 2, 011
- Lovell M. R., et al., 2012, *MNRAS*, 420, 2318
- Ludlow A. D., et al., 2016, preprint, ([arXiv:1610.07663](https://arxiv.org/abs/1610.07663))
- Lundgren A. P., Bondarescu M., Bondarescu R., Balakrishna J., 2010, *ApJ*, 715, L35
- Madau P., Shen S., Governato F., 2014, *ApJ*, 789, L17
- Magaña J., Matos T., Robles V., Suárez A., 2012, *Journal of Physics Conference Series*, 378, 012012
- Marsh D. J. E., 2016, *Phys. Rep.*, 643, 1
- Marsh D. J. E., Pop A.-R., 2015, *Mon. Not. Roy. Astron. Soc.*, 451, 2479
- Marsh D. J. E., Grin D., Hlozek R., Ferreira P. G., 2014, *Phys. Rev. Lett.*, 113, 011801
- Martínez-Medina L. A., Matos T., 2014, *Mon. Not. Roy. Astron. Soc.*, 444, 185
- Martínez-Medina L. A., Robles V. H., Matos T., 2015a, *Phys. Rev. D*, 91, 023519
- Martínez-Medina L. A., Bray H. L., Matos T., 2015b, *JCAP*, 1512, 025
- Matos T., Guzman F. S., 2000, *Class. Quant. Grav.*, 17, L9
- Matos T., Robles V. H., 2016, preprint, ([arXiv:1601.01350](https://arxiv.org/abs/1601.01350))
- Matos T., Rodríguez-Meza M. A., 2014, *Journal of Physics Conference Series*, 545, 012009
- Matos T., Suarez A., 2011, *Europhys. Lett.*, 96, 56005
- Matos T., Ureña-López L. A., 2000, *Classical and Quantum Gravity*, 17, L75
- Matos T., Ureña-López L. A., 2001, *Phys. Rev.*, D63, 063506
- Matos T., Ureña-López L. A., 2007, *Gen. Rel. Grav.*, 39, 1279
- Matos T., Guzmán F. S., Ureña-López L. A., 2000, *Class. Quant. Grav.*, 17, 1707
- Matos T., Vázquez-González A., Magaña J., 2009, *MNRAS*, 393, 1359
- McGaugh S. S., 2005, *The Astrophysical Journal*, 632, 859
- McGaugh S. S., de Blok W. J. G., Schombert J. M., Kuzio de Naray R., Kim J. H., 2007, *ApJ*, 659, 149
- McGaugh S., Lelli F., Schombert J., 2016, preprint, ([arXiv:1609.05917](https://arxiv.org/abs/1609.05917))
- Membrado M., Pacheco A. F., Saáúdo J., 1989, *Phys. Rev.*, A39, 4207
- Monachesi A., Bell E. F., Radburn-Smith D. J., Bailin J., de Jong R. S., Holwerda B., Streich D., Silverstein G., 2016, *MNRAS*, 457, 1419
- Moore B., Quinn T., Governato F., Stadel J., Lake G., 1999, *MNRAS*, 310, 1147
- Navarro J. F., Frenk C. S., White S. D. M., 1997, *Astrophys. J.*, 490, 493
- Navarro J. F., et al., 2010, *MNRAS*, 402, 21
- Núñez D., González-Morales A. X., Cervantes-Cota J. L., Matos T., 2010, *Phys. Rev. D*, 82, 024025
- Pawłowski M. S., Pflamm-Altenburg J., Kroupa P., 2012, *Mon. Not. Roy. Astron. Soc.*, 423, 1109
- Pawłowski M. S., et al., 2014, *MNRAS*, 442, 2362
- Peebles P. J. E., 2000, *ApJ*, 534, L127
- Planck Collaboration et al., 2016, *Astron. Astrophys.*, 594, A13
- Pontzen A., Governato F., 2012, *MNRAS*, 421, 3464
- Pontzen A., Governato F., 2014, *Nature*, 506, 171
- Press W. H., Ryden B. S., Spergel D. N., 1990, *Phys. Rev. Lett.*, 64, 1084
- Robles V. H., Matos T., 2012, *Mon. Not. Roy. Astron. Soc.*, 422, 282
- Robles V. H., Matos T., 2013a, *Phys. Rev. D*, 88, 083008
- Robles V. H., Matos T., 2013b, *ApJ*, 763, 19
- Robles V. H., Lora V., Matos T., Sánchez-Salcedo F. J., 2015, *ApJ*, 810, 99
- Rodríguez-Montoya I., Magaña J., Matos T., Pérez-Lorezana A., 2010, *ApJ*, 721, 1509
- Rubin V. C., 1983, *Science*, 220, 1339
- Rubin V. C., Ford W. K. J., Thonnard N., 1980, *ApJ*, 238, 471
- Sahni V., Wang L., 2000, *Phys. Rev.*, 62, 103517
- Sarkar A., Mondal R., Das S., Sethi S., Bharadwaj S., Marsh D. J., 2016, *Journal of Cosmology and Astroparticle Physics*, 2016, 012
- Sawala T., et al., 2016, *MNRAS*, 457, 1931
- Schive H.-Y., Chiueh T., Broadhurst T., Huang K.-W., 2016, *ApJ*, 818, 89
- Schive H.-Y., Chiueh T., Broadhurst T., 2014a, *Nature Phys.*, 10, 496

- Schive H.-Y., Liao M.-H., Woo T.-P., Wong S.-K., Chiueh T., Broadhurst T., Hwang W. Y. P., 2014b, *Phys. Rev. Lett.*, 113, 261302
- Sin S.-J., 1994, *Phys. Rev.*, D50, 3650
- Smith S., 1936, *ApJ*, 83, 23
- Spergel D. N., Steinhardt P. J., 2000, *Physical Review Letters*, 84, 3760
- Suárez A., Chavanis P.-H., 2016, preprint, ([arXiv:1608.08624](https://arxiv.org/abs/1608.08624))
- Suarez A., Matos T., 2011, *Mon. Not. Roy. Astron. Soc.*, 416, 87
- Suárez A., Robles V. H., Matos T., 2014, *Astrophysics and Space Science Proceedings*, 38, 107
- Teyssier R., Pontzen A., Dubois Y., Read J. I., 2013, *MNRAS*, 429, 3068
- Ureña-López L. A., Bernal A., 2010, *Phys. Rev. D*, 82, 123535
- Ureña-López L. A., González-Morales A. X., 2016, *JCAP*, 7, 048
- Walker M., 2013, *Dark Matter in the Galactic Dwarf Spheroidal Satellites*. Springer Science+Business Media Dordrecht, p. 1039, [doi:10.1007/978-94-007-5612-0_20](https://doi.org/10.1007/978-94-007-5612-0_20)
- Weinberg D. H., Bullock J. S., Governato F., Kuzio de Naray R., Peter A. H. G., 2015, *Proceedings of the National Academy of Science*, 112, 12249
- Wetterich C., 2001, *Physics Letters B*, 522, 5
- Woo T.-P., Chiueh T., 2009, *ApJ*, 697, 850
- Yoshida N., Springel V., White S. D. M., Tormen G., 2000, *ApJ*, 544, L87
- Zavala J., Jing Y. P., Faltenbacher A., Yepes G., Hoffman Y., Gottlöber S., Catinella B., 2009, *ApJ*, 700, 1779
- Zhao H., 1996, *Mon. Not. Roy. Astron. Soc.*, 278, 488
- Zwicky F., 1933, *Helvetica Physica Acta*, 6, 110
- Zwicky F., 1937, *ApJ*, 86, 217
- de Blok W. J. G., McGaugh S. S., Rubin V. C., 2001a, *AJ*, 122, 2396
- de Blok W. J. G., McGaugh S. S., Rubin V. C., 2001b, *Astron. J.*, 122, 2396

This paper has been typeset from a \LaTeX file prepared by the author.